ACCURACY ASSESSMENT OF REAL-TIME KINEMATICS (RTK) MEASUREMENT ON UNMANNED AERIAL VEHICLES (UAV) FOR DIRECT GEO-REFERENCING

DESTA DAWIT EKASO
February 2018

SUPERVISORS:
Prof.dr. Norman Kerle
Dr.Francesco Nex
Advisor:
Dr.Siavash Hosseinyalamdary

ACCURACY ASSESSMENT OF REAL-TIME KINEMATICS (RTK) MEASUREMENT ON UNMANNED AERIAL VEHICLES (UAV) FOR DIRECT GEO-REFERENCING

DESTA DAWIT EKASO
Enschede, The Netherlands, February 2018

Thesis submitted to the Faculty of Geo-Information Science and Earth Observation of the University of Twente in partial fulfilment of the requirements for the degree of Master of Science in Geo-information Science and Earth Observation.
Specialization: Natural Hazards, Risk and Engineering

SUPERVISORS:
Prof.dr. Norman Kerle
Dr.Francesco Nex
Advisor:
Dr.Siavash Hosseinyalamdary

THESIS ASSESSMENT BOARD:
prof.dr. V.G. Jetten (Chair)
Prof. Markus Gerke (External Examiner, Technical University of Braunschweig,Germany)

DISCLAIMER
This document describes work undertaken as part of a programme of study at the Faculty of Geo-Information Science and Earth Observation of the University of Twente. All views and opinions expressed therein remain the sole responsibility of the author, and do not necessarily represent those of the Faculty.

ABSTRACT

During the natural hazard events such as flooding, earthquake, and tsunami, a rapid response is needed for rescue missions, and remote sensing-based disaster response system plays a great role in this area in mitigating the hazard as well as in post-disaster recovery management stages. Geospatial information of accurate location based on the unmanned aerial vehicle (UAV) provide valuable information in this regard to support decision-making system. This research aims to evaluate the accuracy of the Real-time kinematics (RTK) Global navigation satellite system (GNSS) on Matrice 600 Pro. Although a very high accuracy of 2 to 3 cm is claimed for GNSS RTK by the manufacturer (DJI company), the actual accuracy of the RTK for positioning the images and for using it for mapping purposes is not known. The aircraft has two GNSS RTK antenna; one is used for heading reference, and the other is used for providing positioning data. The GNSS RTK reference center or the reading location of the positioning unit in the drone was not clearly stated by DJI company neither does the commercial drone companies know the reference point. In this study, the reference center is determined through experimental studies using the dual frequency Leica GNSS with RTK capability. The RTK positioning data from the drone are then used for direct georeferencing, and its results are evaluated. Custom made synchronization module is used to match the images with the positioning data. The physical set up of the GNSS antenna and the camera system has shown large lever arm offset, and this is calibrated using physical measurements and 3D transformation of the positional information. The flight is carried out in the 70x70 m test area with an altitude of 40 m above the ground with a ground sampling distance (GSD) of 1.3 cm. The indirect method of aerial triangulation is used as a reference system for camera position and to assess the quality of directly georeferenced camera positions. The results of direct georeferencing for the photogrammetric product has shown a decimetre level accuracy. Evaluated against the check points, the planimetric accuracy ranges between 30 to 60 cm for the three experiments. The direct comparison of GNSS RTK reading with the GCP assisted aerial triangulation has resulted in a relatively higher RMSE error both in the planimetric and vertical directions. The analysis of the achieved direct georeferencing result with a velocity of the aircraft revealed that the time delay between the GNSS RTK and camera image acquisition and this caused the higher error for the obtained direct georeferencing results. Based on the obtained results, the general overview is given on its implication and sufficiency for natural hazard application.

Keywords: UAV, GNSS RTK, direct georeferencing, aerial triangulation, GNSS RTK, lever arm offset.

ACKNOWLEDGEMENTS

I would like to thank God who helped me during my education and my stay in the Netherlands.

I would also like to thank the Netherlands government who funded my education and my stay through NFP program and without their support this would not have been possible.

My supervisors, Prof.dr. N. Kerle and Dr. F.C. Nex played a great role in sharing their knowledge and giving me constructive comments, and I would like to express my sincere gratitude for their unconditional support they gave me during my study period in ITC. Their support was very helpful for me both during lectures and research phases.

My advisor Dr. S. Hosseinyalamdary was very supportive of me in giving me comments and ideas during my research work, and I am very grateful for his support.

I am also grateful to Ir. B.G.C.M. Krol for being there to talk to during the core module and throughout my study in ITC. Both as a lecturer and as a course director he had a positive influence on me. I am indebted to all of the teachers of Applied earth science department in ITC for teaching and sharing their knowledge with us.

I would like to take this opportunity to thank my parents, my brothers and sisters for their moral support throughout my study.

Last but not least, my thanks and appreciation go to all of my classmates and my friends for making my stay in the Netherlands wonderful and memorable.

TABLE OF CONTENTS

LIST OF FIGURES

LIST OF TABLES

LIST OF APPENDIXES

1. INTRODUCTION

1.1. Motivation and problem statement

Satellite-based positioning is used to determine the position of observation sites on the ground. Signals from operational satellites of Global Navigation Satellites Systems (GNSS) such as GPS, BDS, GALILEO and GLONASS are tracked by GNSS receivers on the ground to calculate their location (Hofmann-Wellenhof, Lichtenegger, & Wasle, 2008a). These GNSS receivers provide measurements with an accuracy of few meters enough for small-scale regional surveying and mapping applications. An improved positioning technique is to use differential GNSS (DGNSS) which can provide very accurate location measurements in the range of few centimeters using two or more receivers (Hofmann-Wellenhof et al., 2008a). Real-time measurements are allowed through this DGNSS technique which are also known as Real-time kinematics (RTK) enabling rapid mapping applications much easier. The use of positioning instruments for aerial surveying has been the focus of many types of research.

Over the years different photogrammetric approaches have been developed for accurate estimation of geographic location using GNSS systems on Unmanned Aerial Vehicle (UAV) (Eisenbeiss, 2004; Eisenbeiß, Zurich, Eisenbeiß, & Zürich, 2009). Due to the limitation of the payload and cost, however, the onboard sensors on UAV are of low quality from which the location information derived contain wider uncertainty. Photogrammetric block adjustments must be done to minimize this error distribution on image blocks acquired through UAVs. Indirect determination of sensor orientation (indirect geo-referencing) is used for this purpose to minimize image block deformation using Ground control points(GCP) (Chiang, Tsai, & Chu, 2012). GCPs are used in bundle adjustment for image location estimation in a geographic coordinate system (Chiang et al., 2012; Pfeifer, Glira, & Briese, 2012). Aerial triangulation is applied when processing multiple images to extract exterior orientation by which homologous points of adjacent images are measured, and a point on the space is determined (Cramer, Stallmann, & Haala, 2000). This method gives an accurate estimation of location and orientation. It has, however, little significance when it comes to rapid mapping applications such as rescue missions since it is time-consuming because of the post-processing. Its implementation is also limited in inaccessible areas where GCP collection is not possible. A large amount of interactive editing, the increased overlap requirement for a stereo generation, and the necessity for GCPs limit the applicability of the indirect method. Though the accuracy obtained is high, its efficiency is poor (Chiang et al., 2012).

The use of Real-time kinematic (RTK) measurement enhances the positioning, giving a more accurate reading of feature locations of up to a 2 cm accuracy (Gerke & Przybilla, 2016). It uses the GNSS carrier phase to modulate signals between satellite and the receiver (Odijk, Zhang, & Teunissen, 2015). The receiver in the base station sends a differential signal to the GNSS receiver in the UAV through communication link and correction is applied by the RTK. The recently released DJI Matrice 600 Pro drone has an RTK unit (also known as D-RTK by the manufacturers as part of the DJI series) onboard, with a dual frequency that can reduce effects from atmospheric delay to help precise positioning and also its ambiguity resolution is much faster when compared to a single frequency. However, the accuracy and precision of its photogrammetric products and its significance for rapid mapping application are not yet known.

Precise measurements are essential for direct geo-referencing to use it for rapid mapping applications and RTK plays a critical role for this purpose. Remotely sensed images from UAV are related to the earth in the case of direct geo-referencing by accurately measuring the position and orientation of the sensors without GCPs (Mostafa & Hutton, 2001). It requires integrated measurement from both GNSS and inertial navigation system (Chiang et al., 2012; Cramer et al., 2000; Mian et al., 2015) for absolute positioning and orientation. Inertial measuring unit (IMU) has poor long-term stability, but it has a very high frequency and supports GNSS measurements (Jacobsen, 2002). Better results can be achieved by this method when RTK is used. In principle, the onboard RTK can provide 2 cm to 3 cm accurate absolute positioning (Gerke & Przybilla, 2016) and along with the attitude measurements from IMU, the location and orientation of the camera can be improved. The main problem is the errors that might be introduced into the system in the process which reduce the accuracy of the measurement.

The source of errors is either because of the incorrect determination of interior orientation parameters or because of the position of the instruments and their operation in the UAV platform where the location of the camera, GNSS, and IMU are different within the platform. Camera calibration is done to obtain correct interior orientation parameters such as principal distance and focal length. The focal length, however, may not be the same for every flight and hence self-calibration is recommended (Rehak & Skaloud, 2017; Skaloud, 1999) in most cases to continuously estimate the focal length.

The misalignment between the IMU and the camera, which is also called the boresight effect, and the physical offset between the IMU and the camera are sources of errors associated with internal set up of the UAV that affects the accuracy of RTK measurement. Another source of error to consider is the effect of time synchronization occurred as a result of the time delay between camera acquisition and GNSS receiver. According to Rehak & Skaloud (2017) for the carrier phase noise of around 2 cm, the time synchronization should be performed better than 1 ms for ground velocities of 10-30 m/s.

The effect of all these errors on the RTK onboard the DJI Matrice 600 Pro, their influence on its photogrammetric product and ways to minimize them, need further investigation. Although some of these effects have been studied by other researchers (Cramer et al., 2000; Gerke & Przybilla, 2016; Ip, 2005; Jacobsen, 2002; Mian et al., 2015; Turner, Lucieer, & Wallace, 2014), their studies are based on light weight multirotor and fixed-wing UAVs. Since the Matrice 600 Pro has the different sensor set up in terms of their placement on the platform, the lever arm, miss-alignment and time delay will also be different. In addition to these, the manufacturers provided very few information about the system, and hence it is necessary to do a detailed study to use the full potential of this drone. The drone is meant to be a survey-grade instrument, yet the accuracy is not well known.

The accuracy of the measurements generated using D-RTK information from this new DJI Matrice 600 Pro, will be evaluated to understand the uncertainty range. The errors can be measured using RMSE between the estimated and measured positions (Gómez-Candón, De Castro, & López-Granados, 2014; Liba and Berg-Jürgens, 2015; Ruzgiene, Berte, Ge, Jakubauskiene, & Aksamitauskas, 2015).

The low-cost solution of using ultra-light UAVs such as DJI phantom does not provide accurate positional measurements for rapid mapping without GCP. The focus of this study is, therefore, to examine whether the Matrice 600 Pro with D-RTK capability can be a solution for rapid mapping applications in natural hazard areas and to see if we can achieve the theoretical 2 cm to 3 cm RTK accuracy without GCPs.

1.1.1. Main Objective

The main goal of this study is to assess the accuracy of RTK measurements on Matrice 600 Pro UAV for direct geo-referencing and to analyze their impact on the resulting photogrammetric products.

1.1.2. Specific objectives and research questions

The following are specific objectives and research questions that are going be addressed by this research:

- Determining the GNSS RTK reference center within the drone
    - Which part of the drone do the GNSS RTK positional values refer to?
- Determining the lever arm offset between the GNSS reference center and the camera center as the camera center moves following the gimbal rotation.
    - What is the lever arm offset or distance between the GNSS receiver and the camera center?

- Performance evaluation of direct geo-referencing and its implication for natural hazard application
    - How accurate are the direct geo-referencing measurement and the resulting photogrammetric product?
    - Are the results obtained from direct geo-referencing sufficient for natural hazard applications?

Thesis structure:

Chapter 1 Introduction: this chapter includes the general introduction to the research idea and the motivation to the study discussed. In addition to that, the research objectives, as well as research questions, are introduced in this part of the chapter.
Chapter 2 Literature review: this chapter has literature review on the subjects related to the objectives of the current research
Chapter 3 The UAV system: this part of the chapter gives the general overview of the UAV components
Chapter 4 Methodology: this chapter includes descriptions of the methodology proposed to answer the research questions.
Chapter 5 Result and discussion: this chapter contains the final result in table and graphical format obtained from this research including the discussion of the results.
Chapter 6 Conclusion and recommendation: the concluding statements were made in this chapter based on the results of the previous chapter.

2. LITERATURE REVIEW

2.1. Satellite-based positioning

Satellite-based positioning is the process of determining the position of observing sites on the land, sea air or in space by using artificially made satellites orbiting the earth (Hofmann-Wellenhof et al., 2008a). The position or location of an object on the ground is calculated using the satellite signal information reaching the receiver. The geometric distance from the receiver to each satellite is determined by recording the travel time of the satellite signal to the receiver (Hofmann-Wellenhof et al., 2008a). Three satellites are needed to calculate the location of an object in space. However, due to the clock offset between the receiver and the satellite, the range estimated in this method will not be the true distance and hence called pseudoranges. Therefore, four satellites are required to avoid this error bias and obtain better positioning information (Hofmann-Wellenhof et al., 2008a) for static receivers. Various satellite navigation systems are under operation currently for positioning purpose including GPS (the US-based Global Positioning System), Galileo (European satellite system), GLONASS (Russian satellite system) and BeiDou (China-based satellite system) and other navigation systems together forming Global Navigation Satellite System (GNSS). Based on the satellite signals from this GNSS satellites, either differential positioning or real-time kinematics can be performed to obtain the location of the receiver on the ground. Differential positioning uses code and carrier-based measurement to calculate a position while real-time kinematic system uses only carrier phase and gives the results in real time (Hofmann-Wellenhof et al., 2008a; Souza, Monico, & Pagamisse, 2009). The basic principle between the two systems, however, is the same in which they both need two receivers to calculate a position and one receiver (base station) is used to correct the measurement of the other receiver (mobile station).

2.1.1. Differential Positioning (DGNSS)

A differential positioning system (DGNSS) determines the position of the moving receiver/the rover based on the correction signal received from the receiver in the base station with a known coordinate. The reference station calculates the pseudorange correction and range rate correction to be sent to the moving rover (Hofmann-Wellenhof et al., 2008a). Assuming the two receivers, one at the base station denoted by (*b)* and the other, the moving receiver, denoted by (*a*), the unknown observables required to determine positioning of receiver (*a)* can be estimated through pseudo range measurement and corrections sent by receiver (*b)* (Hofmann-Wellenhof et al., 2008a; Morales & Tsubouchi, 2007).

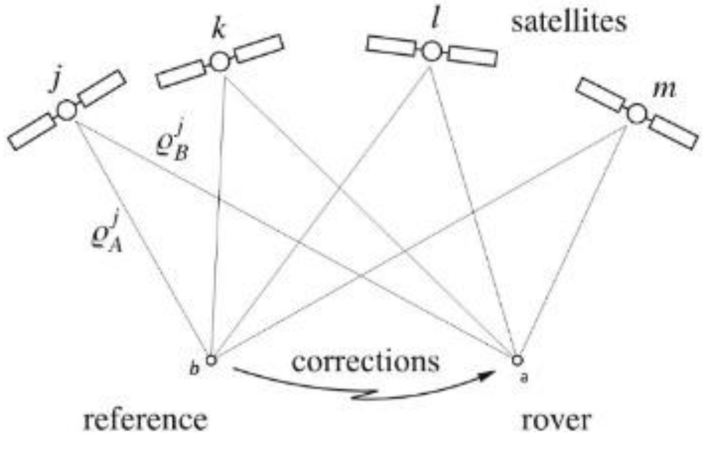

Figure 2-1: Basic concepts of differential positioning

2.1.1.1. Code based measurement

The GNSS receiver generates code replica of the satellite signals. The code signal generated by the GNSS receiver and the code signal transmitted by the satellite are compared by the GNSS receiver. As described by Spockeli, (2015), the equation for code pseudorange measurement is given by:

$$R_a^j = \boldsymbol{\rho} + \boldsymbol{c}\Delta\delta(t) \quad (1)$$

Where R_a^j is the Pseudorange from the satellite and the receiver, $\boldsymbol{\rho}$ is the distance between the receiver and the satellite in the transmission time, epoch t, c is the speed of light, $\Delta\delta$ is the clock bias from the satellite (δ_j) and the receiver (δ_a) i.e. $\Delta\delta$(t)= δ_a(t) - δ_j(t). Because of the high stability atomic clock measurement, (δ_j) is small and can be modelled using the coefficient transmitted in the navigation message. The receiver clock offset (δ_a) however is large and treated as unknown variable to be determined from the above equation of pseudorange.

The geometrical range $\boldsymbol{\rho}$ between the satellite and receiver can be computed from the satellite position (Xj, Yj, Zj) at transmission time, t and from the receiver position (Xa, Ya, Za) (Kouba, 2009; Souza et al., 2009)

$$\rho = \sqrt{(Xj - Xa)^2 + (Ya - Yj)^2 + (Zj - Za)^2} \quad (2)$$

2.1.2. Real-time kinematics (RTK)

Real-time kinematics GNSS system provides real-time positioning information with a real-time correction giving a very high accurate measurement in a centimeter level (Morales & Tsubouchi, 2007; Xu, 2012). GNSS RTK receives satellite signal with two receivers. One of the two receivers is used as a base station with a known coordinate, and the other is a mobile station. The base station records the location of its position and sends a correction signal to the mobile station to correct the location signal recorded by the mobile receiver or rover. This system requires a communication channel to communicate between the two ground receivers. The strength of the communication signal reduces as the distance between the receivers increases and it is not valid anymore if the receivers are too far apart. RTK system is therefore subject to communication barriers, and it may not work well in urban areas where buildings might block the signal preventing the communication of the receivers.

The advantage of using RTK is that it ensures fast determination of ambiguity resolution (fixed solution) (Xu, 2012). GNSS RTK provides two kinds of solutions; the float and fix (Morales & Tsubouchi, 2007; Xu, 2012). The float solution provides low accuracy results of around 20 cm up to 1 m and is based on a minimum of four satellites to define the location, while the fixed solution requires five common satellites and provides positioning information with an accuracy of less than 2 cm. RTK mainly uses carrier based phase measurement to obtain position information, and it is more accurate than code based measurement. The phase range is determined by calculating the number of carrier cycles between the satellite and the receiver

2.1.2.1. Phase measurement

To determine the phase range, the number of cycles between the satellite and the receiver needs to be added to R_a^j (equation 1):

$$\lambda\Phi = \boldsymbol{\rho} + \boldsymbol{c}\Delta\delta + \lambda N \quad (3)$$

Similar to the code measurement, $\boldsymbol{\rho}$ is the true distance from the satellite to the receiver on the ground, c is speed of light, $\Delta\delta$ is the clock bias, λ is the wavelength of the satellite signal, and N is the number of cycles also known as phase ambiguities.

2.1.2.2. Ambiguity resolution

To get a high accuracy measurement, the ambiguity has to be resolved. The systematic errors such as clock errors, atmospheric refraction, and orbital errors should be removed.

2.1.2.3. Single differencing

This is when the two receivers (*a* and *b*) on the ground receive a signal from a single satellite (*s*) in space. i.e., two receivers and one satellite. In single differencing, errors related to the satellite such as orbit errors and satellite clock bias are considered to be the same for the observations from the two receivers, and therefore they are canceled out (Souza et al., 2009). The phase range of single differencing between the receivers is given by:

$$\lambda\Phi^{j}_{ab} = \Delta\rho^{j}_{ab} + c\Delta\delta_{ab} + \Delta\mathcal{E}^{j}_{ab} + \lambda\Delta N^{j}_{ab} \tag{4}$$

Where, $\boldsymbol{\Delta\rho^{j}_{ab}}$ is the true range from the satellite, *j* to the receivers a and b, $c\Delta\delta_{ab}$ is clock bias in the two stations, $\Delta\mathcal{E}^{j}_{ab}$ is a term for error sources such as random noise and multipath, ΔN^{j}_{ab} is the ambiguity difference in the two receivers coming from satellite *j*.

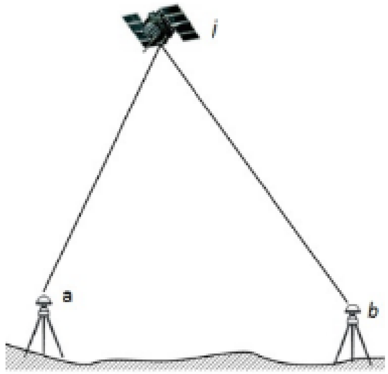

Figure 2-2: Single differencing (Souza et al., 2009)

2.1.2.4. Double differences

Double differencing considers the signals from the two satellites *i* and *j* received by the receivers *a* and *b*. They are determined from two single differences, and this eliminates the receivers clock biases (Hofmann-Wellenhof et al., 2008a; Souza et al., 2009; Walpersdorf, Bouin, Bock, & Doerflinger, 2007). The elimination of receivers clock bias is the main reason for double differencing, and it is given by:

$$\lambda\Phi^{ij}_{ab} = \Delta\rho^{ij}_{ab} + \Delta\mathcal{E}^{ij}_{ab} + \lambda\Delta N^{ij}_{ab} \tag{5}$$

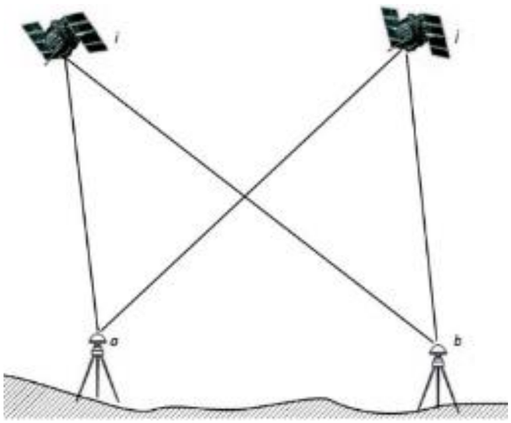

Figure 2-3: Double differencing (Souza et al., 2009)

2.1.2.5. Biases and noises

Pseudorange measurements obtained by code and phase measurements are affected by biases and random noise factors. These errors sources are mainly satellite related, propagation medium related and the receiver related causes. The satellite related error sources are satellite clock bias and orbital errors. Ionospheric and tropospheric refraction are error sources related to satellite signal propagating medium between the receiver and the satellite. Errors associated with receivers on the ground include antenna phase center variation, clock bias and multipath effects (Hofmann-Wellenhof et al., 2008a). Some of the systematic errors can be removed or at least be reduced by differencing measurements between the receivers or satellites (Kouba, 2009). Single differencing between the receivers and a single satellite removes satellite related error sources and double differencing between two satellites, and a single receiver eliminates receiver related biases (Hofmann-Wellenhof et al., 2008a).

2.1.2.6. Multi-path effects

This effect is caused by multiple reflections of the satellite signal (Hofmann-Wellenhof et al., 2008a; Rost & Wanninger, 2009). The incoming satellite signal, in principle, arriving at the receiver is direct. However this direct satellite signal is superimposed by indirect signal reflected in the antenna surroundings, and this causes the phase of the received signal to be shifted when compared to the directly received signal (Rost & Wanninger, 2009). The effects of multipath can be reduced by proper selection of sites for receivers which are protected from signal reflections caused by surroundings such as buildings, trees, and vehicles (Hofmann-Wellenhof et al., 2008a). Since multipath is wavelength dependent, carrier phase measurements are less affected by it when compared to code measurements (Hofmann-Wellenhof et al., 2008a).

2.1.2.7. Atmospheric effects

The most common atmospheric effects that influence the propagation of satellite signals are the ionospheric and tropospheric effects. The troposphere extends to about 50 km from the earth surface, and its refraction index is a function of mainly temperature, pressure, and partial water vapor pressure (Hofmann-Wellenhof et al., 2008a). Most of the tropospheric delay is caused by dry or hydrostatic parts which are mainly a function of pressure (Hofmann-Wellenhof et al., 2008a). The ionosphere is electrically charged part of the atmosphere that refracts the incoming GNSS signal. The effect of ionosphere varies with time (day and night) because the ionization of the ionospheric layer varies with the sun light. According to Hofmann-Wellenhof et al., 2008a, the ionized gases in the ionospheric layer of the atmosphere causes the electromagnetic waves to shift and the effect of this cases the code pseudoranges to become longer and phase pseudoranges to be shorter. These atmospheric effects can be greatly reduced if the base line distance between the receivers is short, (no more than 20 km) (Souza et al., 2009) and the differencing mechanisms (i.e., single differencing and double differencing) are the techniques to remove/reduce these biases (Hofmann-Wellenhof et al., 2008a; Kouba, 2009; Souza et al., 2009).

2.1.2.8. Clock bias

In satellite-based positioning, information from the three or more satellites is needed to get a positional fix for the receiver. But small errors or drifts in the clocks highly affect the positioning of the receiver in the space because satellite clocks and the receiver clocks are not synchronized accurately. The atomic clocks of the satellites are very accurate, but a small drift in the timing affect the positioning of the receiver. A drift in terms of nanosecond can cause tens of meter shift from the true position. The bigger error, however, comes from the receiver clock because of its low accuracy. This makes the synchronization with satellite clock impossible. Therefore, additional unknown clock bias needs to be introduced, and hence four satellites are needed to solve for this unknowns (Hofmann-Wellenhof et al., 2008a).

While the ionospheric and tropospheric effects on the arriving signals are mitigated and effectively done for shorter distance particularly less than 20 km and the orbital errors of less than 100 km, the satellite clock errors are cancelled out using the differencing techniques no matter how long the base length distance is (Al-Shaery, Zhang, & Rizos, 2013). According to Al-Shaery et al., (2013) this reduces the amount of errors that need to be estimated for effectively resolving integer ambiguity. Double differencing of the GNSS observables can eliminate satellite clock bias (Walpersdorf et al., 2007) which applies differencing technique between the two receivers and the two satellites.

2.1.2.9. Satellite orbit errors

In addition to the effects of clock bias, atmospheric errors and multipaths, orbital errors influence the 3D poisoning of the receivers. Therefore, precise satellite orbits must be known to analyze the GNSS data and accurately estimate the receiver position. Precise satellite orbits are obtained from international GNSS service (IGS)(Hofmann-Wellenhof et al., 2008a; Rost & Wanninger, 2009). The IGS also provides other corrections terms such as satellite clock error corrections, ionospheric and tropospheric correction values calculated from hundreds of permanent networks worldwide. The IGS final calculated orbital solution is less than 5 cm average precision and hence the orbital errors no longer represent major error source for post-processing (Rost & Wanninger, 2009).

For single receiver positioning, the orbital error is highly correlated with positional errors and with respect to base lines, the relative orbital error is approximately the same with relative baseline error (Hofmann-Wellenhof et al., 2008a; Rost & Wanninger, 2009).

2.2. UAV based satellite positioning and geo-referencing

Positioning and navigation devices mounted on UAVs are used to determine the location and orientation of features on the ground as well as the location of the platform itself on the space (Bryson & Sukkarieh, 2015). GNSS and IMU sensors are used in this case for geographic location and attitude determination of the imaging sensor. GNSS sensors mounted on the drone track the satellite signals to determine their positional information while flying. There sensors are mainly positional and attitude sensors. The GNSS sensors help to locate the drone on the space and the attitude sensors such as IMU record the orientation information while the UAV is flying. The other sensors, compasses, are used to determine the heading references with respect to the magnetic north.

2.2.1. Indirect Geo-referencing

Among many other applications of drones, they are used for mapping purposes for monitoring the ground features using the mounted cameras. This follows geolocating each image taken by the camera. Since the GNSS sensors on the drone are not very accurate, error follows the geolocation process and the photogrammetric products will not be accurate, resulting uncertainties in meters. In order to minimize this effect, ground control points are taken using the survey grade GNSS measurement units, and the image blocks are adjusted. The GNSS measurements are used for initial approximation to align the images. Indirect geo-referencing uses aerial triangulation (AT) for adjusting a network of tie points in a block of images with ground control points on the ground (Ip, 2005). Interior and exterior orientation parameters of the images are determined during the AT process. This is expensive procedure when large areas are to be considered and especially when the areas are inaccessible because of the need to collect ground control points correct referencing.

2.2.2. Direct geo-referencing with RTK GNSS

Indirect geo-referencing is time-consuming. In addition to that, accessing ground control point is difficult in areas of natural hazards such as flooding, forest fires, earthquake distraction sites, etc. and hence, the ability to obtain exterior orientation parameters through aerial triangulation is impossible. Such situations requiring rapid response need fast orthophoto generation to address the resulting problem, and there are insufficient time and resources to extract external orientation parameters using aerial triangulation (Ip, 2005). The increasing technological advances in the field of mapping and photogrammetry have allowed the direct geo-referencing solution on UAV to turn into an effective way for rapid mapping.

Direct geo-referencing provides the ability to directly relate the data collected through UAV to the Earth by measuring the GNSS position and attitude of the drone without using ground control points (Ip, Mostafa, Hutton, & Barriere, 2008; Rehak, Mabillard, & Skaloud, 2013). This facilitates the process of mapping works by providing the accurately referenced images and location of features right away without the need to post-process the images and hence reduces the time it used to take to map the area during indirect geo-referencing approach. A very accurate GNSS sensor reading and IMU measurements are required for direct geo-referencing to get appropriate results. The integrated approach of combining GNSS and IMU measurement is used in most cases by researchers to generate accurate mapping products. GNSS has long time stability, but IMU has poor long-time stability, and at the same time IMU provides a very high-frequency measurement, and therefore they support each other when combined together (Jacobsen, 2002). The technique used for UAV based direct geo-referencing module developed by Chiang, Tsai, & Chu (2012) makes use of the integrated approach incorporating the sensor readings from low-cost Micro Electro Mechanical System (MEMS) inertial navigation system (INS) and GNSS. Unlike the traditional method of aerial triangulation which uses an interpolation within an area of the control points, direct geo-referencing extrapolates from the projection centres to the ground, and therefore the steps involved in this method should be handled with more care than the indirect approach (Jacobsen, 2002).

In order to do direct geo-referencing with sufficient accuracy, any navigation system providing orientation and positioning information has to fulfil the following three conditions according to (Skaloud, 1999): i) The position and orientation offset between the imaging sensor and navigation sensor has to be determined with sufficient accuracy, ii) this position and orientation offset should remain constant or otherwise its variation has to be modelled ii) the imaging, position, and orientation sensors have to be synchronized to a common time base with a sufficient accuracy.

Recent developments in the field of the aerial survey included the integration of RTK device with the aircraft which will be used for direct assignment of the camera position or exterior orientation parameters from the RTK reading with very high accuracy. By making this possible survey grade, direct sensor positioning of UAV images became a reality. Unlike the Differential GNSS usually mounted on the drone which considers only code based measurements, the onboard RTK unit incorporates phase measurements which provide absolute accuracy in the range of centimeter (Gerke & Przybilla, 2016). Therefore, given that the theoretical high accuracy of GNSS RTK solution onboard, other error sources such as delay due to improper camera synchronization, the physical positional difference between the GNSS and the camera, and also the angular misalignment between the two sensors are the causes of errors or uncertainties in direct georeferenced photogrammetric products and should be done accurately in order to get the overall high oriented block imagery for mapping purpose.

2.2.2.1. Camera synchronization

In direct geo-referencing, the synchronization of the records of the camera time and the GNSS time needs to be done precisely because no optimization is done to minimize this kind of error, unlike the traditional aerial triangulation. Therefore accurate time tagging of the camera shutter precisely with the GNSS time scale is a precondition for direct geo-referencing in order to correlate the orientation and position data correctly with the recorded images (Rehak et al., 2013). The requirements for time synchronization increases with accuracy requirements and the aircraft dynamics. Sensor synchronization is a serious source of error and directly affect the positioning information obtained by the aircraft if done incorrectly (Skaloud, 1999). The degree of error increases with the speed of the aircraft. One millisecond (1ms) synchronization error can affect the position and orientation recordings of the sensors by about 10 cm for the aircraft velocity of 360 km/h or 100 m/s (Skaloud, 1999) for a fixed wing aircrafts. Multi rotary small copters, however, travel at a much lower speed. Turner et al. (2014) fitted a flash sync unit to the camera's hotshoe adapter and then connected to GNSS unit to record precise camera shutter pulse in the GNSS log file. In this developed system, when the camera shutter is opened, a pulse is sent to the GNSS and time stamped with a precision of 0.001 s. According to Turner et al. (2014), for the camera with a shutter speed of 1/200th of a second, the maximum delay between a shutter and a flash pulse is 0.005s, and with a maximum drone speed of 5 m/s, the resulting inaccuracy is around 2.5 cm and the positional error caused by time synchronization delay is insignificant in this case.

2.2.2.2. Coordinate systems and angles used in inertial navigation

There are various coordinate systems whose axis and centre of origin are different from one another. The different types of coordinate systems are described as follows (Chapala, Pirati, & Nelakuditi, 2016; Zhang, Ghogho, & Yuan, 2012): i) Body coordinate system (b-frame): the origin of its axis is the centre of the aircraft. The x-axis points in the forward direction of the aircraft, the y-axis points to the right side and the z-axis point downward. ii) Inertial coordinate system (i-frame): the origin of the axis is the centre of the Earth, and their non-rotating axes are fixed ones. iii) Earth coordinate system (e-frame): the origin of this axis is the centre of the Earth, and their non-rotating axes are aligned with respect to the Earth. iv) Navigation coordinate system (n-frame): it is the local geographic navigation frame with its location at the center of the navigation system itself. They are aligned in the east (x), in the north (y) and vertical up (z-axis) also called the 'ENU frame'. v) Wander azimuth navigation system (p-frame): Like the n-frame, it is of a local level but rotates through the wander angle (with respect to the north) about the local vertical.

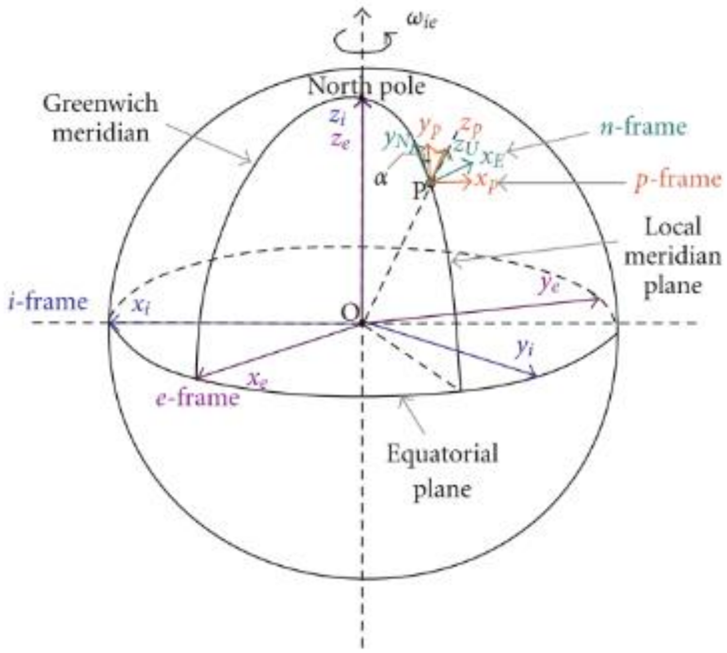

Figure 2-4: Reference frames (Zhang et al., 2012)

The definitions of axis and angels obtained from the inertial reference system are different from those coordinate systems and angles (omega, phi, and kappa) needed for geo-referencing and hence appropriate transformations must be done (Bäumker & Heímes, 2001). For mapping products from direct geo-referencing, special attention should be given for data obtained from inertial systems of the aircraft because of the difference in the coordinate system and the transformation equations used for coordinate transformations (body coordinate to navigation system) are based on the angles from this inertial system. For example, the lever arm from the camera to the GNSS is measured in the body coordinate systems (b-frame) and needs to be transformed into navigation coordinate system (n-frame) using the roll, pitch and yaw angles from the inertial systems. The transformation matrix ($\boldsymbol{C_b^n}$)used for the transformation is calculated in the order of (Bäumker & Heímes, 2001): 1st rotation around the x-axis, R_x (roll, $\boldsymbol{\phi}$); 2nd rotation around the y-axis, R_y (pitch, $\boldsymbol{\theta}$) and ; 3rd rotation around z-axis, R_z (yaw, $\boldsymbol{\psi}$) or heading. The combination of the three rotations results in the following orthogonal transformation matrix:

$$\boldsymbol{C}_b^n = \boldsymbol{R}_z(\psi)\cdot\boldsymbol{R}_y(\theta)\cdot\boldsymbol{R}_x(\phi) = \begin{bmatrix} \cos\psi & -\sin\psi & 0 \\ \sin\psi & \cos\psi & 0 \\ 0 & 0 & 1 \end{bmatrix} \cdot \begin{bmatrix} \cos\theta & 0 & \sin\theta \\ 0 & 1 & 0 \\ -\sin\theta & 0 & \cos\theta \end{bmatrix} \cdot \begin{bmatrix} 1 & 0 & 0 \\ 0 & \cos\phi & -\sin\phi \\ 0 & \sin\phi & \cos\phi \end{bmatrix}$$

$$\boldsymbol{C}_b^n = \begin{bmatrix} \cos\psi\cdot\cos\theta & \cos\psi\cdot\sin\theta\cdot\sin\phi - \sin\psi\cdot\cos\phi & \cos\psi\cdot\sin\theta\cdot\cos\phi + \sin\psi\cdot\sin\phi \\ \sin\psi\cdot\cos\theta & \sin\psi\cdot\sin\theta\cdot\sin\phi + \cos\psi\cdot\cos\phi & \sin\psi\cdot\sin\theta\cdot\cos\phi - \cos\psi\cdot\sin\phi \\ -\sin\theta & \cos\theta\cdot\sin\phi & \cos\theta\cdot\cos\phi \end{bmatrix}$$

2.2.2.3. Lever arm

The differences between the exterior orientation parameters derived from a conventional aerial triangulation and exterior orientation parameters obtained directly from integrated IMU and GPS reading are used for lever arm calibration (Lo et al., 2015). The location of the GPS antenna with respect to the camera position is fixed and therefore the distance difference between the GPS antenna and the camera can be measured directly in the roll, yaw and pitch axis defined by the onboard IMU unit of the drone which is obtained from the log files (Turner et al., 2014). They compared the photogrammetric products produced applying lever arm correction and without applying the correction to evaluate the effect of lever arm offset and realized that the spatial accuracy has decreased to 19 cm from 11.5 cm for the generated orthomosaic image without applying the lever arm correction. Therefore, it is necessary to apply lever arm correction when working with direct geo-referencing.

Two-step approach was implemented by Chiang et al. (2012) to determine the lever arm offset between the IMU and the camera centre. The first step was to calculate the exterior orientation parameters though bundle block adjustment by measuring the image location. The second step was to interpolate the integrated IMU/GNSS measurements at each image exposure time. The lever arm offset was then obtained by comparing the exterior orientation parameters from the two measurements. The quality of the determined vector distance is dependent on the flight altitude and flight dynamics according to Chiang et al. (2012) that it decreases with decreasing the flying height of the aircraft. However, ground control points are needed for this kind of lever arm estimation. The lever arm estimated by Rehak et al. (2013) was done by just using a caliper, and the results were then compared with the lever arm determined through bundle adjustment using ground control points. The result of the comparison shows very closer similarity with a slightly higher difference along the y-axis.

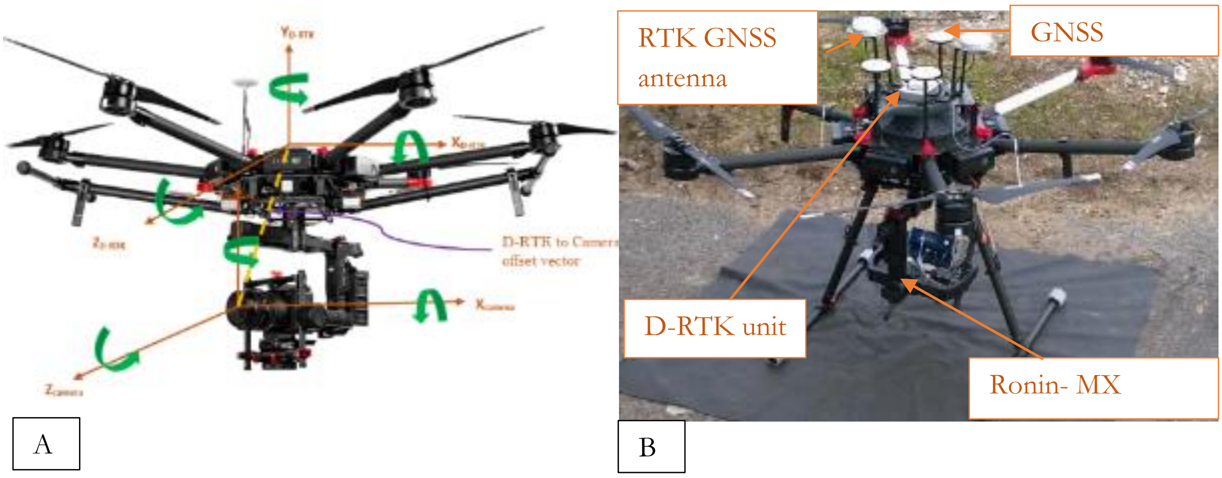

Figure 2-5: UAV system: A) Physical offset (lever arm) from D-RTK to the camera. B) D-RTK, GNSS antenna and gimbal set up in the UAV system.

2.2.2.4. Boresight

For accurate measurements using direct geo-referencing, careful estimation of miss-alignment between IMU and the camera needs to be done. The boresight misalignment happens because of the imperfect alignment between camera or the imaging sensor and the IMU during the hardware integration (Ip, 2005). The IMU system is fixed to the camera body but its axis may not be parallel to the camera axis, and this requires the determination of the relation between the two axes together with the offset of both systems origin (Jacobsen, 2002). This is done by comparing the IMU rotation axis with the rotation of controlled block adjustment (Jacobsen, 2002). For boresight angle determination, the reference images should be carefully selected. The first and the last images covering the study area partially are not recommended for a reference image for boresight calibration (Jacobsen, 2002). The methods used to compute boresight calibration angles for direct geo-referencing are discussed by in Skaloud (1999), and Mostafa & Hutton (2001b) are summarized by Ip (2005) as follows:

- Comparing the IMU/GPS derived angles with those independently computed angles from aerial triangulation and the constant difference between the angles considered as the three components of the boresight angles.
- Computing the boresight angles as additional unknown parameters in the bundle block adjustment assisted by IMU/GPS values.

In the first method, the IMU-derived attitude matrix are compared to that of photogrammetrically derived attitude matrix and then averaging the boresight angles over a number of images is done in a block configuration for accurate calibration according to Mostafa & Hutton (2001). The second method is more flexible and efficient because of the fact that the GPS/IMU assisted block adjustment procedure can be done without ground control points (Ip, 2005).

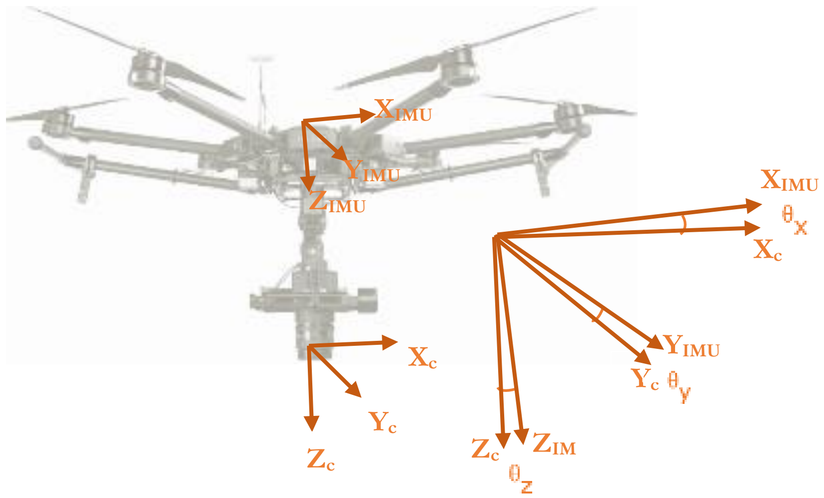

Figure 2-6: Concept of boresight angles or angle misalignment

2.3. Accuracy of photogrammetric products from direct geo-referencing

The accuracy of ground feature coordinates when using direct geo-referencing depends on the GPS accuracy for positioning and IMU accuracy for attitude (Ip, 2005). The orientation error due to the IMU accuracy causes position error as a function of the flying height of the aircraft (Ip, 2005). The accuracy of direct geo-referencing is mostly done through ground control points distributed in the study area. The direct geo-referencing coordinates of the check points are compared with their reference points to assess the accuracy of photogrammetric products generated (Lo et al., 2015; Turner et al., 2014).

Hutton, Lipa, & Lutes (2014) performed accuracy assessment of direct georeferenced image products by measuring the misregistration of ground features between the images using quantum GIS because of the insufficient ground control points. Each ground feature is measured in all available photos, and for each point, the mean positional error is calculated from all images, and the error is finally estimated by comparing against the mean position resulting in a total RMSE of 14 cm. The study result of Turner et al. (2014) for the absolute spatial accuracy of the photogrammetric products created using direct geo-referencing method is around 11 cm. This is done using 22 ground control points distributed in the study area and single frequency onboard GNSS measurements integrated into the system.

The accuracy of direct geo-referencing (UAV RTK only solution) performed by Gerke & Przybilla, (2016) using the onboard real-time kinematic module placed on the fixed wing aircraft shows better results (

around 5 cm) when compared to the normal built-in GNSS which is in meters. The accuracy of absolute orientation of the image blocks on this study enhanced when using the onboard RTK unit. According to Gerke & Przybilla, (2016), UAV RTK solution delivers results which are better than the traditional indirect sensor orientation.

2.4. Summary

UAV based positioning and mapping have been the focus of various researches, and the advancement of the technology helped ease the tedious process of traditional mapping. Different types of UAVs have been deployed to improve the quality of mapping products. The purpose of this study is, therefore, to evaluate the accuracy of industrial drone (i.e., Matrice 600 Pro) for mapping application particularly in the area of natural hazards.

3. THE UAV SYSTEM

This part of the chapter is meant to give the general overview of the UAV system employed in this study. The discussion of the capability of UAV, its sensors, and other parts of the UAV which can affect the quality of the final mapping product is included here.

3.1. The redundancy system

The system has a flight controller providing triple modular redundancy with three IMU and three GNSS units for accurate estimation of the position and orientation. The redundant mechanism of this system ensures the reliability of navigation information received by the drone. It applies a voting system whereby the majority of observations of the sensor is taken as the correct measurements, and the erroneous measurements are excluded from the observations. The fault-tolerant capacity of the system is, therefore, higher having three attitude sensors and three position sensors with a total of six modular redundancy.

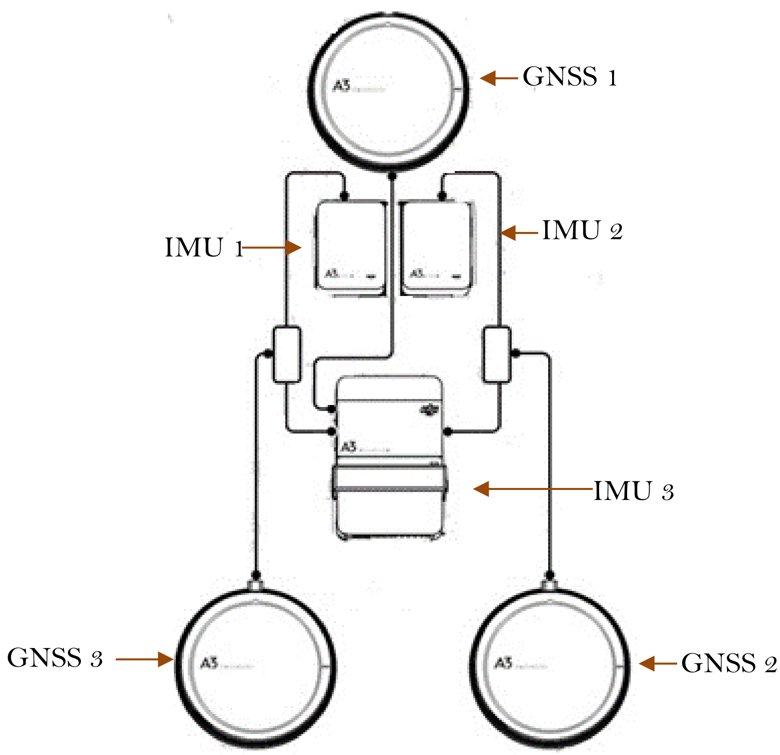

Figure 3-1: Mounting position of the sensors in the UAV system (Modified after DJI user manual, 2016)

3.1.1. The sensors

The sensors onboard the UAV are the attitude sensors such as GNSS receiver, IMU, and the optical sensor which is Canon EOS camera (Canon 600D) placed in the Ronnin MX gimbal front for image acquisition. The GNSS receiver has two categories, the redundant three antennas for position measurements and the two antennas for differential measurements (GNSS RTK) to ensure real-time correction through the datalink placed between them to facilitate communication with the base station. The communication of the GNSS sensors with the A3 pro flight controller has carried out through extended DJI CAN 1 port of the GNSS and the same CAN-Bus (CAN 1) plugin in the flight controller.

The three GNSS-compass modules installed in the UAV systems are aligned in such a way that the red orientation arrow in this positioning device is pointed to the aircraft's nose, and they are oriented along the x-axis given the body coordinates of the aircraft. The mounting position of the first GNSS (GNSS 1) is on the positive axis towards the nose while the second and the third GNSS (GNSS 2 and 3) are in the negative x-axis. The first and third units are placed in the negative y-axis, while the second is in the positive axis. Their dimension is indicated in Table 3-1. The negative Z-axis indicate its position above the center of gravity (COG) of the aircraft according to the default body coordinates set by DJI.

Table 3-1: The mounting position of the GNSS antennas on the aircraft

	GNSS 1	GNSS 2	GNSS 3
X (mm)	129	-102	-102
Y (mm)	-5	59	-52
Z (mm)	-182	-166	-166

The onboard IMU pro unit in the aircraft has a built-in attitude recording sensor and a pressure sensor for detecting a change in aircraft attitude while flying. It has a USB port connected to it with CAN 1 Bus port through which communication is made with GNSS units in the drone. The IMU units are placed on top of the drone's upper plate.

3.2. Vibration absorber

This vibration absorber is placed below the lower plate of the aircraft to reduce the effect of aircraft vibration on the imaging sensor. The gimbal of the aircraft is connected to the main body with this vibration absorber through a circular connector in the middle of the absorber.

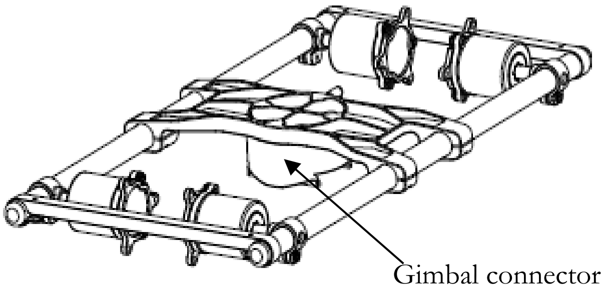

Figure 3-2: Vibration absorber (DJI user manual Ronin-MX, 2016)

3.3. Battery system

The aircraft has six intelligent flight batteries slotted into the battery compartments in the side part of the system to increase the flight time. It has a capacity of 4500mAh and a voltage of 22.2V which help to sustain the longer flight time. The intelligent batteries have a built-in battery management system that assesses the power level of all the batteries when one battery is powered on to evaluate the safety of the power supply and turns on the other batteries if the power supply, as well as its position, is right.

3.4. D-RTK unit

D-RTK is a GNSS-barometer system placed on top of the aircraft above the upper plate to ensure high accuracy positioning of the system. It includes two GNSS units of equal antenna heights. One of the two antennae is the master antenna (ANT 1), and the other (ANT 2) is the slave antenna. ANT 1 is mainly for positioning and ANT 2 is for heading reference. The base distance between the two air system antenna is

25 cm, and they are equidistant from each other when measured from the center. The air system is connected to the base station through datalink pro installed both on the air system and the ground system of D-RTK unit. The antenna unit of the ground system is connected to the D-RTK unit through the antenna cable and the D-RTK device is again connected through the 8-pin cable to the datalink pro on top of it which in turn communicates with the air end. The base station should normally be placed around 10-meter distance or more from the aircraft before takeoff in order to be properly linked with aircraft D-RTK. The RTK system is normally sensitive to any blockade because of the communication channel needed to modulate the correction signal for accurate observation of the air system.
The absolute orientation of the base station needs to be inserted, and it is measured through a very accurate differential GNSS or RTK capable geodetic GNSS systems. The absolute location then needs to be updated by pressing the update button in D-RTK unit.

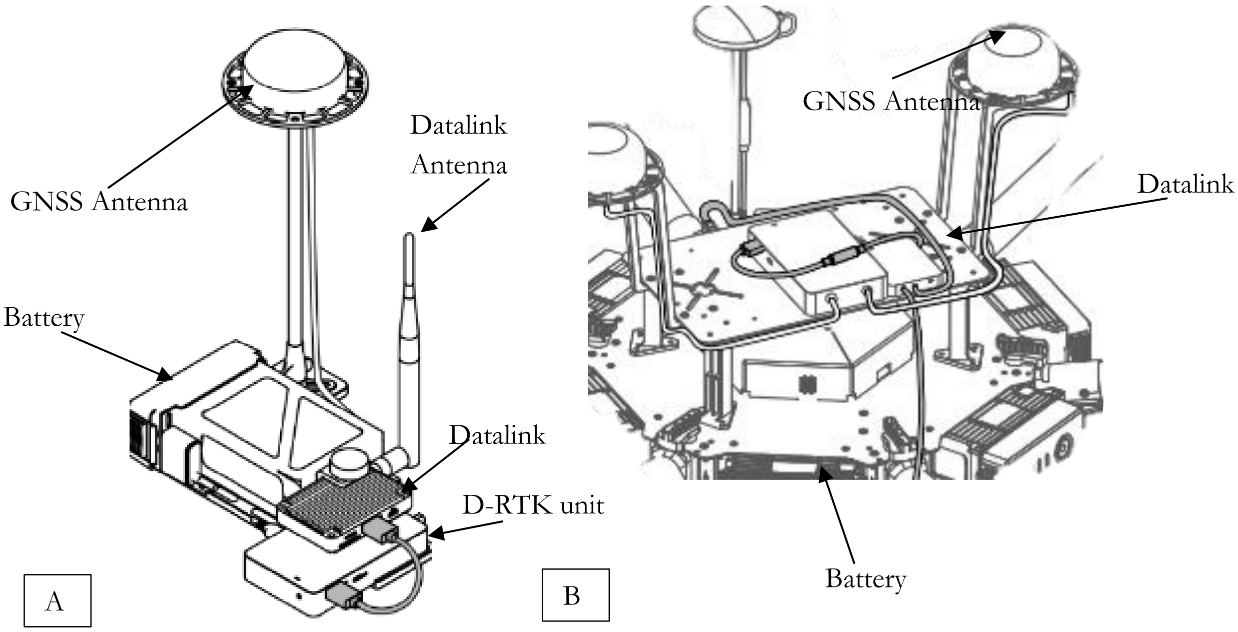

Figure 3-3: D-RTK components A) Ground system B) Air system (DJI user manual Datalink Pro, 2016).

3.4.1. Communication link

The communication between the base station and the aircraft is established through the datalink above the D-RTK unit on both ends. The unit has a single antenna (datalink pro 900 antenna x1) attached to the interface on its side to pass through the signals (Figure 3-3). Unless it is used in an open environment with no blockades, the communication channel will not be established with the air end. Therefore, the location of flight or study area must be carefully chosen to get full functionality and full advantage of the RTK navigation.
The maximum distance that the datalink pro can still have communication is around 5km and therefore the closer the aircraft is to the base station, the better information flow will be developed between the two ends. However, it must not be too close to the station (less than 10 m). To set up the right connection for the D-RTK, the 4-position switch on the datalink pro has to be on the UART-SW1 position on both ground, and air systems and the LED light of the status indicator has to show solid green referring to RTK fixed solution.

3.5. Ronnin-MX gimbal

This is the gimbal system designed to hold the camera and stabilize its movement as the aircraft moves during flight or for handheld use (Figure 4-6). The Ronin MX has a separate IMU unit installed in it to monitor its movement. It is attached to the main body through the vibration absorber of the aircraft beneath the lower plate to help decrease the effect of vibration in the imaging sensor. The gimbal movement is controlled through a 2.4 GHz remote-controller and can rotate it in the desired direction through the two small controller stick.

The Ronnin-MX can be adjusted into a mode known as a smooth track. Smooth track mode is an intelligent gimbal movement prediction system that allows the camera to follow the rotation direction of the gimbal especially when the gimbal is rotating around the z-axis. Disabling the smooth track mode in the remote controller setting will help the camera maintain its position irrespective of the gimbal movement. For aerial imaging, the continuous movement of the camera affects the quality of the images, and it makes feature extraction very difficult. Therefore, it is better this mode is kept disabled when taking images during an aerial survey.

3.6. GNSS/camera synchronization module

The external company known by the name dronexpert.nl has developed a camera triggering module for the drone which will synchronize the recorded GNSS RTK position information and the image from the camera. The module starts to trigger and record GNSS RTK position after the activation height. The activation height can be adjusted in the module to a desired height above the ground.

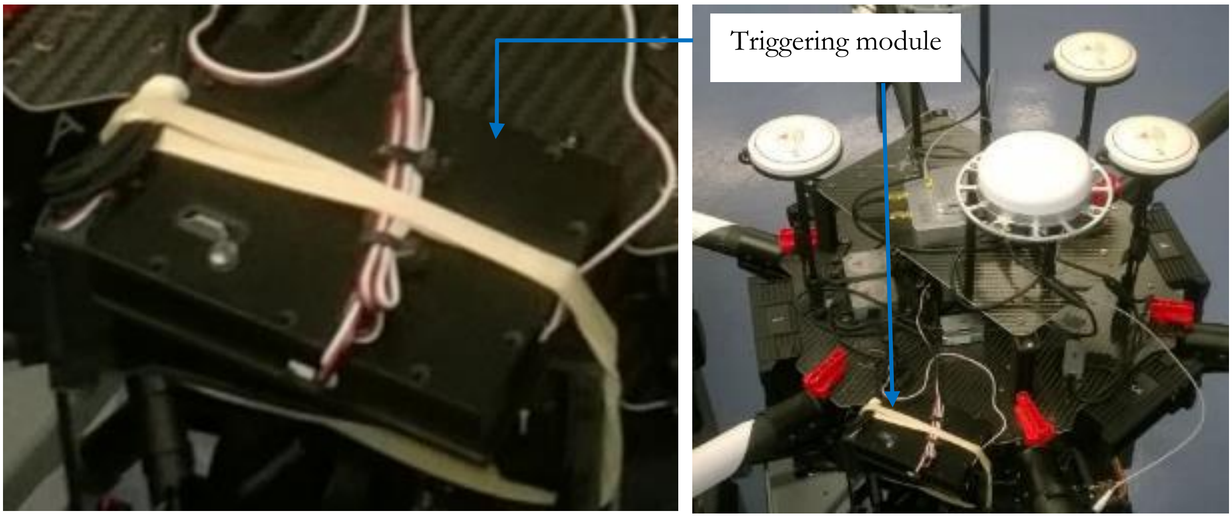

Figure 3-4: GNSS/camera synchronization module (Triggering module)

3.7. Camera properties

The camera used in this research is a compact, lightweight Canon EOS 600D camera. Its properties are described in Table 3-2 and Table 3-3.

Table 3-2: Camera model and its properties

Model	Sensor (Width x Height)(mm)	Resolution (pixel)	Shutter speed (sec)
Canon EOS 600D	22.3 × 14.9 mm	18 mega pixels	1/400 second

Table 3-3: Initial intrinsic camera properties

Principal point (x and y respectively) (mm)	Focal length (mm)	Image (Width x Height)
11.49 and 7.66	20	3456x2304 pixel

3.8. Data flow structure

The position and attitude sensors in the UAV system collect the information needed to locate the aircraft on the space as well as its orientations which later will be used to produce georeferenced photogrammetric products when geotagged or correlated with the image taken from the UAVs imaging sensor (the camera). The structure of data flow in the UAV system is depicted in Figure 3-5 below.

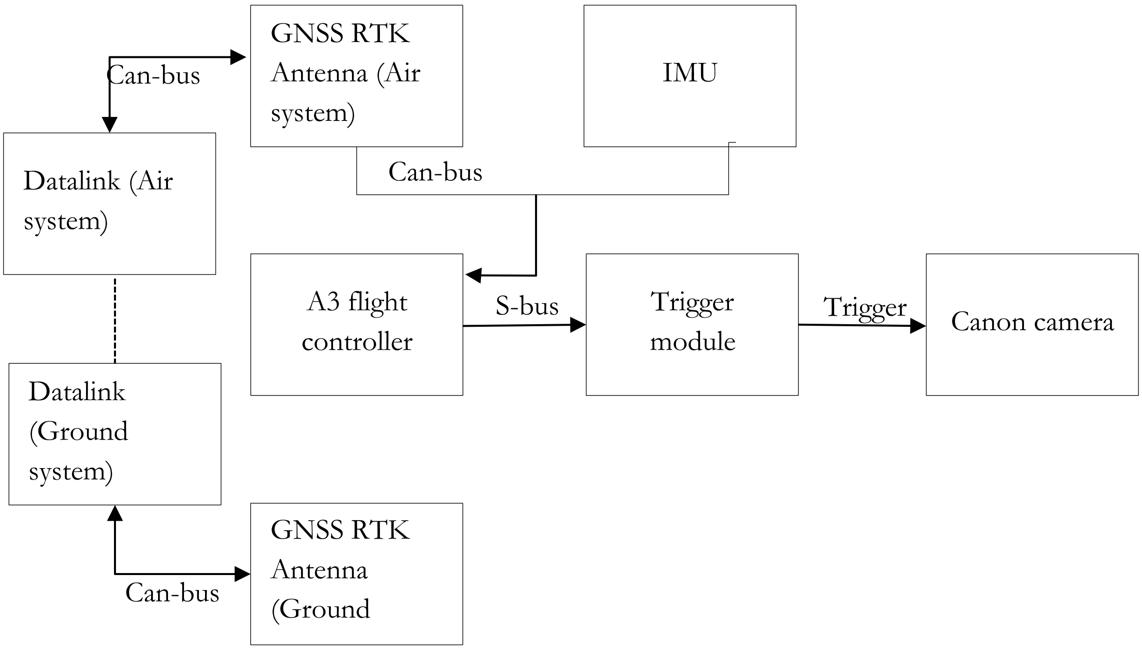

Figure 3-5: Data flow structure in the drone system

3.9. Summary

The drone system used in this study is the latest product of DJI company meant for industrial applications. It has the latest sensors, the gimbal system, vibration absorber and other systems of the drone that will enhance the process of aerial surveying. The information from the sensors flows through the cable systems either through can-bus or s-bus. Positioning and attitude data are finally stored in the flight controller, while images are stored in the SD card of the camera which will be used later for post-processing.

4. METHODOLOGY

The methods used to achieve the proposed studies are briefly described in this chapter. Three main experimental studies are conducted to locate RTK reference center followed by 3D transformations techniques for lever-arm estimation, and finally, evaluation of the accuracy of the mapping products is done to see if it fits the purpose for natural hazard applications.

4.1. Study area

Two study sites were considered for this research. The first area is the parking lot in the backyard of ITC building chosen for the implementation of experimental study for the location of GNSS RTK reference center determination in the drone and the second area was to carry out a test flight, and it is found in Bentelo around 13 km west of Enschede. The first area covers around 600 square meters and the second area covers the area of 5000 square meters.

Figure 4-1: Study area for A) The experimental studies B) Test flights

4.2. Point location of GNSS RTK reference center in the drone

The GNSS reading from D-RTK unit is used to determine the precise location of the drone when performing the aerial survey. However, locating the drone itself is not enough since the RTK GNSS exact reading location is not well known within the drone. Especially for applications that require a very high accuracy this point needs to be identified. The exact location of the reading centre must be known to help locate the imaging sensor (camera). An experimental study was proposed to determine the precise centre of the GNSS RTK measurement location within the drone. Three major experiments were conducted for this purpose in the backyard of ITC building.

4.3. Description of the experimental studies

The three experiments conducted followed a different approach in trying to estimate the drone RTK reference center. The base station was set up 15 m from the UAV location. GNSS locations of all the base stations, as well as the drone locations, were taken with the high accuracy survey grade GNSS RTK with an accuracy (standard deviation of 3D error) of about 0.6 cm. The onboard D-RTK unit on the Matrice 600 Pro by default records the relative location of its point in space with respect to the established base station. In other words, the relative distance of the drone is calculated in the x, y, and z-direction with respect to the base station receiving a correction signal calculated in the base station. The absolute location of the base station was therefore, needed to locate the UAV in space exactly. The survey grade Leica GNSS RTK system was used for absolute location, and its value was entered in the base station. The proposed approach is that the RTK reading of the UAV recorded is compared with the geodetic GNSS RTK at that same place and the difference or the deviation from the geodetic GNSS is the location of UAV RTK reference center.

4.3.1. Measurement with GNSS receiver on the Antenna pole

The UAV (Matrice 600) was placed in the selected location. The location of the two legs of the drone were marked on the ground in the four ends and the centre of the drone was projected down to the ground through the gimbal centre attached to the main body of the aircraft and then the point on the ground was marked. The recording was taken from the flight controller through the USB cable. Real-time corrected measurement of the same location was recorded using GNSS RTK rover of Leica Geosystems. A total of twenty measurements were taken, and the results were compared with measurements from the drone.

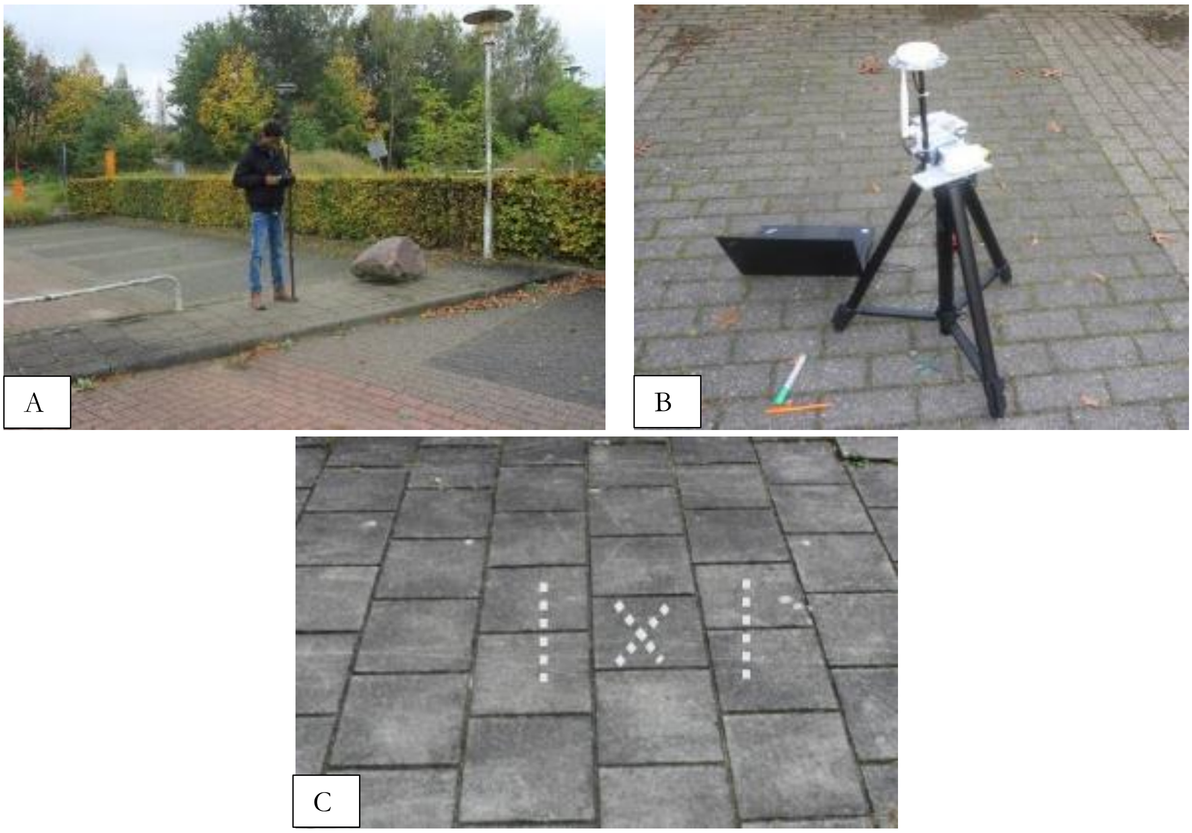

Figure 4-2: Setup of the first experiment A) Measurement of the Geodetic GNSS B) Base station setup for UAV C) Drawing a marker for placing the UAV and the static GNSS.

The correction signal is sent from the base station through a communication link of datalink pro on the UAV system. The absolute location of the base station was measured by GNSS RTK rover, and its value was inserted into the ground system using DJI assistant 2 software from the computer through USB cable. Twenty separate measurements were taken using GNSS RTK rover, and the average value was considered for base stations to minimize uncertainty in a single reading.

4.3.2. Measurement with GNSS receiver on top of the drone

The same base station location was chosen as for the first experiment, and the same absolute location was assigned to the D-RTK following the same procedure in the first experiment. The GNSS antenna of the rover was placed on the datalink device on top of the aircraft carefully balancing and maintaining the horizontality of the ground. This reduces the error (uncertainties) induced when measuring the position while holding the antenna pole by hand. Placing the rover antenna on top of the air end D-RTK unit, however, blocks the communication signal with the base station. Therefore, after the measurement was taken, the antenna was removed from the top of the drone to avoid the error source that might be introduced due to the signal blockage. A total of 22 measurements were taken from this area and the results were assessed.

Figure 4-3: Setup of the second experiment A) Geodetic GNSS placed on the drone B) Horizontal bubble level maintaining the stability.

4.3.3. Measurement with GNSS receiver on tripod

The third experiment was conducted by using a tripod to place the GNSS antenna to stabilize and maintain the horizontality when taking a measurement. Besides its stability, a tripod helps to accurately mark a point on the ground through its lenses, and this is used for setting up base station more precisely (Figure 4-4 A). A total of 20 measurements were taken from the geodetic GNSS RTK receiver and from the D-RTK unit on the drone. The measurements were averaged, and the results were obtained by subtracting the measurement from the geodetic GNSS RTK and from the drone. The experiment was done in two nearby locations using a similar approach.

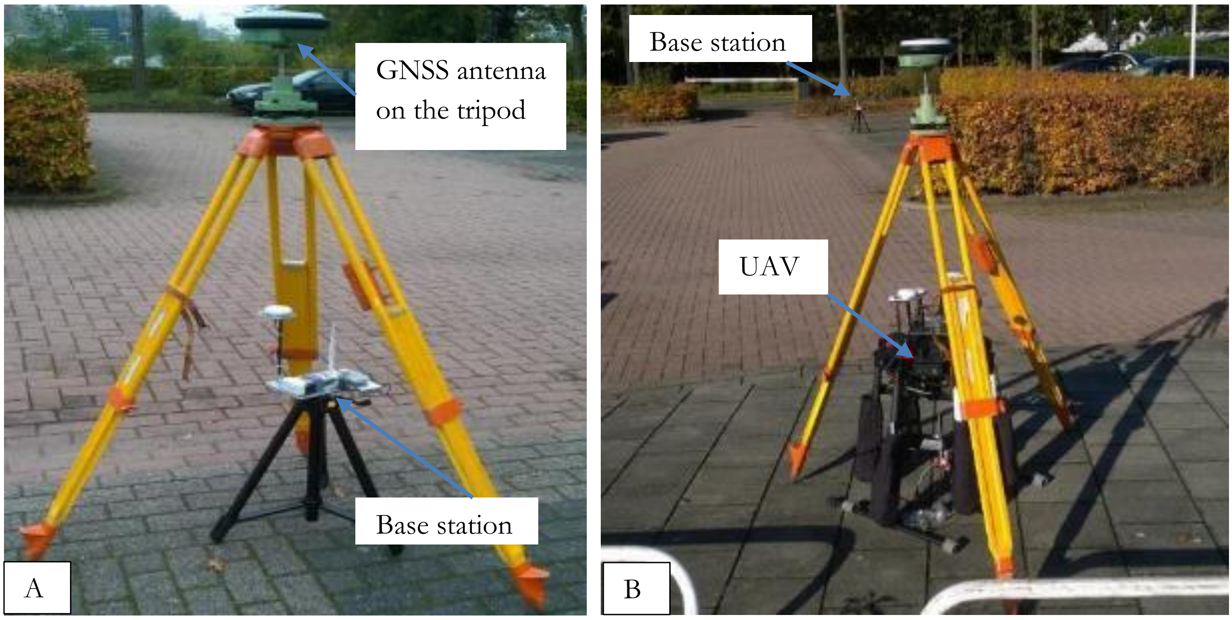

Figure 4-4: A) Base station setup through tripod B) UAV measurement setup using tripod marking the center in the UAV.

4.4. Proposed method for lever arm correction

Direct geo-referencing requires the determination of the transformation vector from the GNSS reference center to the camera lens center. Unlike indirect geo-referencing, which uses the 3D points of the ground (GCPs) to optimize and determine the camera lens center, direct geo-referencing totally depends on the measurements of the positional and orientation sensors for camera location, and hence the quality of final product depends on the accuracy of the positioning of the camera lens center with respect to the GNSS reading center (see Section 2.2.2.3). In our case, Matrice 600, this gap is large and needs to be properly transformed to the camera lens center. There are two parts of transformation to complete the steps. The first part is the main body of the aircraft (absolute transformation) and the second part is the transformation around the gimbal system (relative transformation with respect the main body part) (see Figure 4-5). The rotation angles of the first part of the aircraft are measured by the IMU units placed on top of the upper plate of the aircraft.

The second part assumes the transformation of a point from the GNSS reading center (determined using experimental studies, see Section 4.3) to the top part of the gimbal point, k (Figure 4-6) and finally to the camera center, point p. The orientation of the gimbal (second part) is represented by three angles the yaw (κ), pitch (ψ) and roll (ω) values which are also called Euler angles from the gimbal IMU. The general equation for roto-translation of a homogeneous coordinates for 3D vectors can be obtained using a 4x4 transformation matrix:

$$\begin{bmatrix} x_k \\ y_k \\ z_k \\ 1 \end{bmatrix} = \begin{bmatrix} r_{11} & r_{12} & r_{13} & t_x \\ r_{21} & r_{22} & r_{23} & t_y \\ r_{31} & r_{32} & r_{33} & t_z \\ 0 & 0 & 0 & 1 \end{bmatrix} * \begin{bmatrix} X \\ Y \\ Z \\ 1 \end{bmatrix} \quad (6)$$

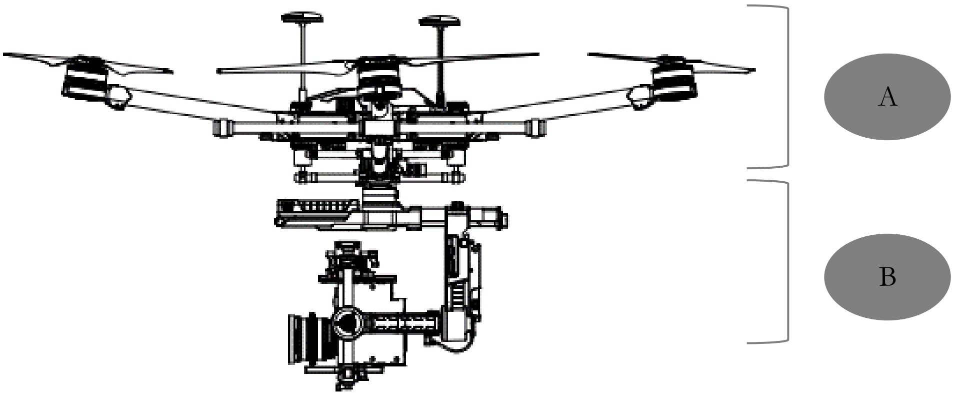

Figure 4-5: The aircraft system, Matrice 600: The main body of the aircraft labeled, A and the gimbal part labeled, B (DJI user manual Matrice 600 Pro, 2016)

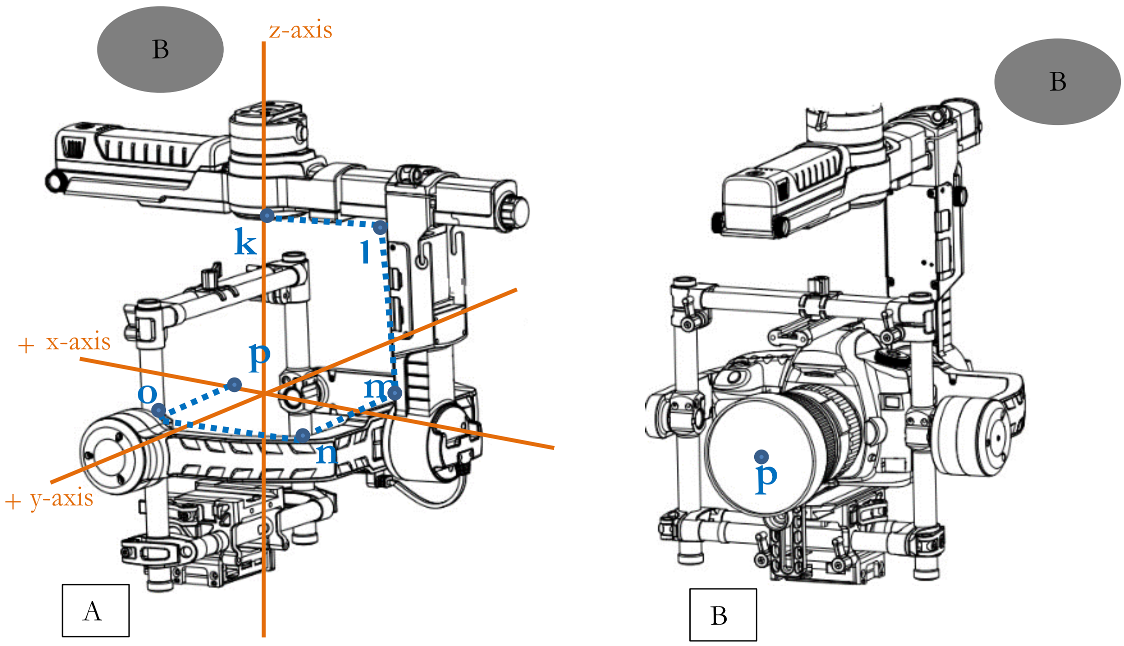

Figure 4-6: Ronin-MX gimbal system A) Transformation points from point, k to the final point, p. B) Gimbal system with a camera installed (DJI user manual Ronin-MX, 2016).

For the sake of convenience, we begin with the second part (Figure 4-6). Assuming there is no rotation in the main body of the drone, part A (Figure 4-5), we can estimate the positional value of the camera lens center at the point, p starting at the top part of the gimbal point, k. In other words, the main body has zero effect on the motion of the gimbal. The rotational procedure followed here is the ZYX; first around the z, axis, then the y-axis and finally around the x-axis and the rotation direction follows the counter-clockwise direction.

Rotation around z-axis (R_κ) is defined using the yaw angle (κ)

$$\mathrm{R}\,\kappa = \begin{bmatrix} \cos\kappa & -\sin\kappa & 0 \\ \sin\kappa & \cos\kappa & 0 \\ 0 & 0 & 1 \end{bmatrix} \tag{7}$$

Rotation around y-axis (R ψ) is defined using the pitch angle, (ψ)

$$\mathrm{R}\,\psi = \begin{bmatrix} \cos\psi & 0 & \sin\psi \\ 0 & 1 & 0 \\ -\sin\psi & 0 & \cos\psi \end{bmatrix} \tag{8}$$

Rotation around x-axis (R ω) is defined using the roll angle, (ω)

$$\mathrm{R}\,\omega = \begin{bmatrix} 1 & 0 & 0 \\ 0 & \cos\omega & -\sin\omega \\ 0 & \sin\omega & \cos\omega \end{bmatrix} \tag{9}$$

The complete roto-translation at the top of the gimbal at point k (Rt_k) from the GNSS reading center is the result of transformation around x, y, and z-axis using the rotation angles from the main IMU unit. Vectors Tk, Tl, Tm, Tn, To, Tp are notations used to represent the 3D translation vectors for points k, l, m, n, o, and p respectively in Figure 4-6 and in the procedure below.

$$\begin{bmatrix} Xk \\ Yk \\ Zk \end{bmatrix} = \mathrm{Rt\_k} = [\mathrm{R}\kappa] * [\mathrm{R}\psi] * [\mathrm{R}\omega] * [\mathrm{T}] + \begin{bmatrix} X \\ Y \\ Z \end{bmatrix} \tag{10}$$

Where X, Y, Z is the original GNSS measurement. Xk, Yk, Zk represent the new points for location, k. T is the 3D translation vector. Therefore, to compute this location (point, k), the transformation is done one by one per rotation axis.

Transformation around x-axis (Rt_x);

Rt_x =R ω * Tk, where R ω is rotation around x-axis, Tk is the 3 D translation vector to point, k

$$\mathrm{Rt\_x} = \begin{bmatrix} 1 & 0 & 0 \\ 0 & \cos\omega & -\sin\omega \\ 0 & \sin\omega & \cos\omega \end{bmatrix} * \begin{bmatrix} Tkx \\ Tky \\ -Tkz \end{bmatrix} = \begin{bmatrix} x \\ y \\ z \end{bmatrix} \tag{11}$$

Transformation around y axis (Rt_y);

Rt_y= R ψ * Rt_x, where R ψ is rotation around y axis, Rt_x is transformation at x

$$\mathrm{Rt\_y} = \begin{bmatrix} \cos\psi & 0 & \sin\psi \\ 0 & 1 & 0 \\ -\sin\psi & 0 & \cos\psi \end{bmatrix} * \begin{bmatrix} x \\ y \\ z \end{bmatrix} = \begin{bmatrix} x' \\ y' \\ z' \end{bmatrix} \tag{12}$$

Transformation around z-axis (Rt_z);

Rt_z= R κ *Rt_y, where R κ is rotation around z-axis, Rt_y is the previous transformation at y

$$\mathrm{Rt\_z} = \begin{bmatrix} \cos\kappa & -\sin\kappa & 0 \\ \sin\kappa & \cos\kappa & 0 \\ 0 & 0 & 1 \end{bmatrix} * \begin{bmatrix} x' \\ y' \\ z' \end{bmatrix} = \begin{bmatrix} x'' \\ y'' \\ z'' \end{bmatrix} \tag{13}$$

Finally, transformation at point, k is equal to: Rt_k= Rt_z+GNSS

$$\mathrm{Rt\_k} = \begin{bmatrix} x'' \\ y'' \\ z'' \end{bmatrix} + \begin{bmatrix} X \\ Y \\ Z \end{bmatrix} = \begin{bmatrix} Xk \\ Yk \\ Zk \end{bmatrix}, \tag{14}$$

Consequently, transformation at point, l (Rt_l);

$$\mathrm{Rt\_l} = \begin{bmatrix} \cos\kappa & -\sin\kappa & 0 \\ \sin\kappa & \cos\kappa & 0 \\ 0 & 0 & 1 \end{bmatrix} * \begin{bmatrix} Tlx \\ Tly \\ Tlz \end{bmatrix} + \begin{bmatrix} Xk \\ Yk \\ Zk \end{bmatrix} = \begin{bmatrix} Xl \\ Yl \\ Zl \end{bmatrix} \tag{15}$$

Rigid body translation at point, m (Rt_m) since there is no rotation component between point, l and m;

$$\text{Rt\_m}=\begin{bmatrix}Xl\\Yl\\Zl\end{bmatrix}+\begin{bmatrix}Tmx\\Tmy\\Tmz\end{bmatrix}=\begin{bmatrix}Xm\\Ym\\Zm\end{bmatrix} \tag{16}$$

Transformation at point, n (Rt_n);

$$\text{Rt\_n}=\begin{bmatrix}1 & 0 & 0\\0 & \cos\omega & -sin\,\omega\\0 & sin\,\omega & \cos\omega\end{bmatrix}*\begin{bmatrix}Tnx\\Tny\\Tnz\end{bmatrix}+\begin{bmatrix}Xm\\Ym\\Zm\end{bmatrix}=\begin{bmatrix}Xn\\Yn\\Zn\end{bmatrix} \tag{17}$$

Rigid body translation at point, o (Rt_o). Again, here there is no rotation component between point, n, and o;

$$\text{Rt\_o}=\begin{bmatrix}Xn\\Yn\\Zn\end{bmatrix}+\begin{bmatrix}Tox\\Toy\\Toz\end{bmatrix}=\begin{bmatrix}Xo\\Yo\\Zo\end{bmatrix} \tag{18}$$

And finally, transformation at point, p (Rt_p) (p is the camera lens center);

$$\text{Rt\_p}=\begin{bmatrix}cos\,\psi & 0 & sin\,\psi\\0 & 1 & 0\\-sin\,\psi & 0 & cos\,\psi\end{bmatrix}*\begin{bmatrix}Tpx\\Tpy\\Tpz\end{bmatrix}+\begin{bmatrix}Xo\\Yo\\Zo\end{bmatrix}=\begin{bmatrix}Xp\\Yp\\Zp\end{bmatrix} \tag{19}$$

The lever arm vector (L_0) is then the difference between the GNSS reading from the GNSS center, $\begin{bmatrix}X\\Y\\Z\end{bmatrix}$ and the transformed vector of the camera location, $\begin{bmatrix}Xp\\Yp\\Zp\end{bmatrix}$.

$$L_0=\begin{bmatrix}X & X_p\\Y-Yp\\Z & Zp\end{bmatrix} \tag{20}$$

However, in reality, the main body of the aircraft (the first part) is in constant motion when flying, and it cannot be zero for the whole duration of the survey. The angles of this part of the aircraft are measured by the redundant main IMU units as mentioned above.

The rotation angles yaw (λ), pitch (ϕ) and roll (θ) obtained from the main IMU unit define the movement of the aircraft. The combination of the three rotation angles results in the orthogonal transformation matrix and transform a coordinate system measured by the main IMU unit to the mapping frame (Cartesian coordinate system) and written as the following:

$$R_b^m = R_\lambda * R_\phi * R_\theta \tag{21}$$

$$R_b^m = \begin{bmatrix}cos\,\lambda & -\sin\lambda & 0\\\sin\lambda & cos\,\lambda & 0\\0 & 0 & 1\end{bmatrix}*\begin{bmatrix}cos\,\phi & 0 & sin\,\phi\\0 & 1 & 0\\-sin\,\phi & 0 & cos\,\phi\end{bmatrix}*\begin{bmatrix}1 & 0 & 0\\0 & \cos\phi & -sin\,\phi\\0 & sin\,\phi & \cos\phi\end{bmatrix} \tag{22}$$

$$R_b^m = \begin{bmatrix}cos\lambda*\cos\phi & \cos\lambda*\sin\phi*\sin\theta-\sin\lambda*\cos\theta & cos\lambda*sin\phi*\cos\theta+\sin\lambda*\sin\theta\\\sin\lambda*\cos\phi & sin\lambda*\sin\phi*\sin\theta+cos\lambda*\cos\theta & sin\lambda*\sin\phi*\cos\theta-\cos\lambda*\sin\theta\\-sin\,\phi & \cos\phi*\sin\theta & \cos\phi*\cos\theta\end{bmatrix} \tag{23}$$

The lever arm (L) in the mapping frame is then determined by applying the transformation matrix on the lever arm vector (L_0) of the gimbal.

$$L = R_b^m * L_0 \tag{24}$$

$$L = R_b^m * \begin{bmatrix}X & X_p\\Y-Yp\\Z & Zp\end{bmatrix} \tag{25}$$

The lever arm vector varies with changing angles of the gimbal as well as the main body, and their values can be estimated from the Euler angles recorded by the gimbal IMU unit and the aircraft IMU units using the above equation (Equation 25).

Based on these equations, a MATLAB procedure has been developed to calculate the different lever arm vectors as per the given yaw, pitch and roll angles from both IMU units. These values are used to adjust the original GNSS measurements and locate the camera projection center used.

4.5. Implementation of Lever arm offset on direct georeferencing

The model developed for lever arm correction of GNSS RTK/camera offset was used for aligning direct georeferenced results obtained from the aircraft. Since the orientation of the aircraft and its gimbal system was changing during the flight, GNSS RTK/camera offset was computed for every image and angle changes observed in the flight data. The offset in the x, y, and z-direction is also determined based on the roll, pitch and yaw angles of both main IMU (aircraft IMU) and the gimbal IMU. The orientation of the aircraft angle was measured in quaternion, and it was converted to Euler angle (see Appendix 1 for conversation equation). The resulting camera position (point, p in Figure 4-6) and the lever arm offset was determined following the stated procedure in section 4.4. GNSS RTK position values of the aircraft were given in degrees (WGS 84 Latitude and Longitude) in the flight log, and it was converted to meters in WGS 84 UTM, and then the offset estimation was made in meters. The final result of the offset is plotted in 2 D graph for better visualization.

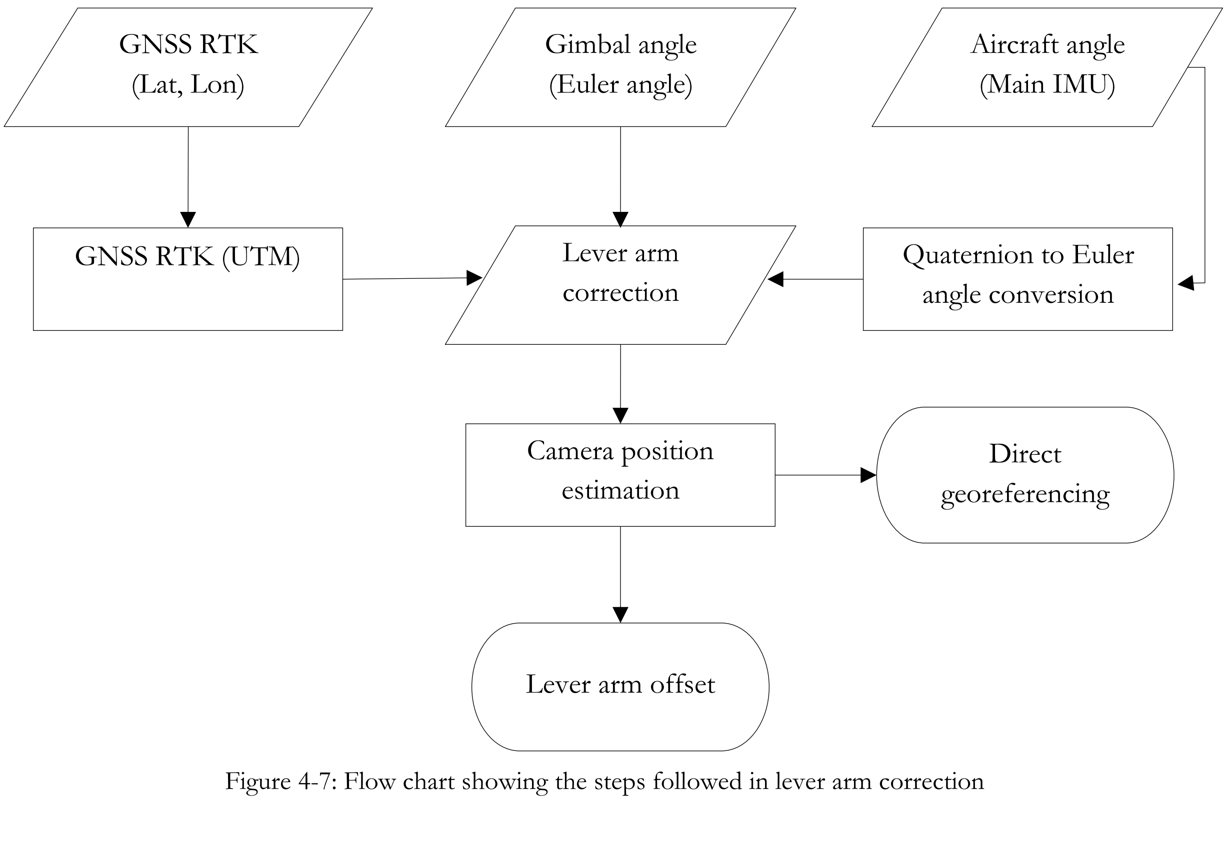

Figure 4-7: Flow chart showing the steps followed in lever arm correction

4.6. Assessment of direct georeferencing

After the calibration for GNSS RTK/camera lens offset, the results of direct georeferencing were evaluated. Two types of evaluation methods were used; the first technique was to compare the camera position obtained from direct georeferencing with the camera position indirectly determined from aerial triangulation. Aerial triangulation was performed with eight evenly distributed ground control points in the study area. The final results of the bundle adjusted camera position were then compared with the direct georeferencing results. The second technique was to run bundle adjustment of the block without GCP using only GNSS RTK direct georeferenced camera position and evaluate its accuracy with control points distributed in the study area.

5. RESULT AND DISCUSSION

The final results obtained using the proposed methods are presented in this chapter. The results of the experimental studies aimed at determining the GNSS reading center in the drone, the GNSS RTK antenna offset and its correction is explained in the second part of this chapter. The accuracy assessment of direct georeferencing based on the indirect approach and the collected control points are explained in detail. Finally, its implication for natural hazard application has been described.

5.1. Results of the experiment

The results of the three experimental studies conducted for the determination of the GNSS RTK reference center are explained in the graphical plot and in the table below.

5.1.1. Results of Geodetic GNSS receiver on the Antenna pole

This was the first attempt to find out the D-RTK reading centre of the drone. The antenna height of the rover was 2 m above the ground, and its value was inserted and corrected for it. GNSS reading in WGS 84 with ellipsoidal height reference was obtained from the system in XML file type and converted into excel sheet. The measurements from the two GNSS units, the geodetic GNSS, and the drone D-RTK were assessed together, and the comparison was made. The results plotted on the graph show that the first experiment conducted has relatively higher variations and uncertainties in representing the location as the antenna pole was held by hand which caused a motion big enough to affect the measurement. The final results obtained by subtracting the geodetic measurement from UAV GNSS (i.e., average values) is 1.9 cm in the East and 1.778 cm in the North from the centre of the drone (Table 5-1). The height component is 2.14 cm above the ground with a standard deviation of 2.47 cm.

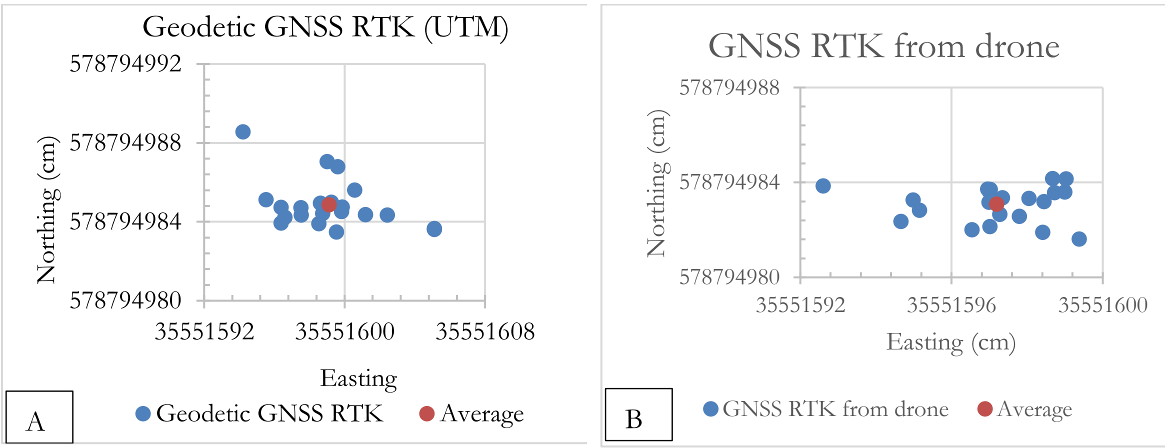

Figure 5-1: Graphical plot of the first experiment A) Geodetic GNSS B) D-RTK from the drone

Table 5-1 Result of the deviation from the geodetic reference measurement in the first experiment

	Easting (cm)	Northing (cm)	Height (cm)
Geodetic	35551599.117	578794984.86	8089.448
UAV	35551597.19	578794983.08	8091.598
Difference (Geodetic and UAV)	1.926	1.778	-2.1494

STD	2.14048	1.204	2.47822

5.1.2. Results of Geodetic GNSS receiver on top of the drone

GNSS measurements of 22 readings were assessed in this part of the experiments where the measurement of geodetic GNSS readings compared with measurements of the same location from the drone RTK. The height of the geodetic GNSS receiver antenna, in this case, was 83.5 cm above the ground and it was taken into account when measuring the location. The readings show clustering around a common value in a better agreement than the first experiment (see Figure 5-2). From the same location, readings were taken from the aircraft RTK. The results in Table 5-2 indicate the difference of about 0.759 cm in the East and 0.61 cm in the North. The vertical height component has a difference of 2.26 cm with a standard deviation of 0.93 cm.

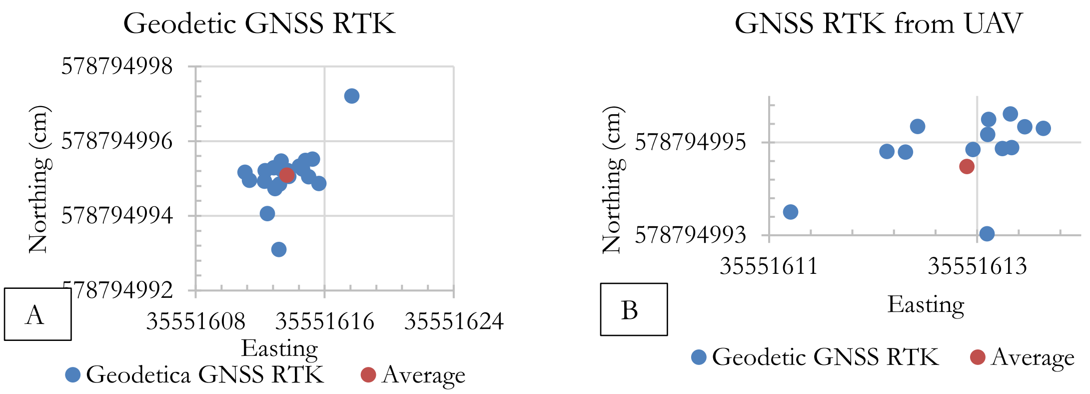

Figure 5-2: Graphical plot of the second test experiment A) From geodetic GNSS B) From the drone.

Table 5-2: Result of the deviation from the geodetic reference measurement in the second experiment

	Easting (cm)	Northing (cm)	Height (cm)
Geodetic	35551613.66	578794995.09	8067.051
UAV	35551612.901	578794994.48	8069.317
Difference (Geodetic and UAV)	0.759	0.6106	-2.2659
STD	1.702753	1.55777	0.936072

5.1.3. Results of Geodetic GNSS receiver on tripod

The horizontal and vertical measurements from the drone and the geodetic GNSS are compared to determine the point location of the D-RTK reading from the drone. A total of 20 continuous measurements were obtained from geodetic GNSS in two close by locations (Location 1 and 2) and the same 20 measurements from the drone. The antenna height from the ground for the geodetic GNSS RTK in the first location was 1.535 m and 1.655 m in the second location. As shown in the graphical plot (Figure 5-3) of the results below both measurements have high precision and clustered towards each other. The measurement accuracy of the geodetic GNSS has a 3D error (standard deviation) of less than 0.7 cm in all measurements. The measurements of both systems are averaged, and the difference between the two systems indicate the deviation of the D-RTK GNSS unit of about -0.47 cm in the horizontal x (Easting) direction and 0.37 cm in the y (Northing) direction from the geodetic GNSS RTK in the first location. Its nearby measurement (Location 2) has a smaller difference in both directions with a value of -0.878 cm in the x-direction and a much smaller difference of 0.044 cm in the y-direction from the geodetic GNSS. The height component has 0.28 and -1.92 in the first and second locations respectively.

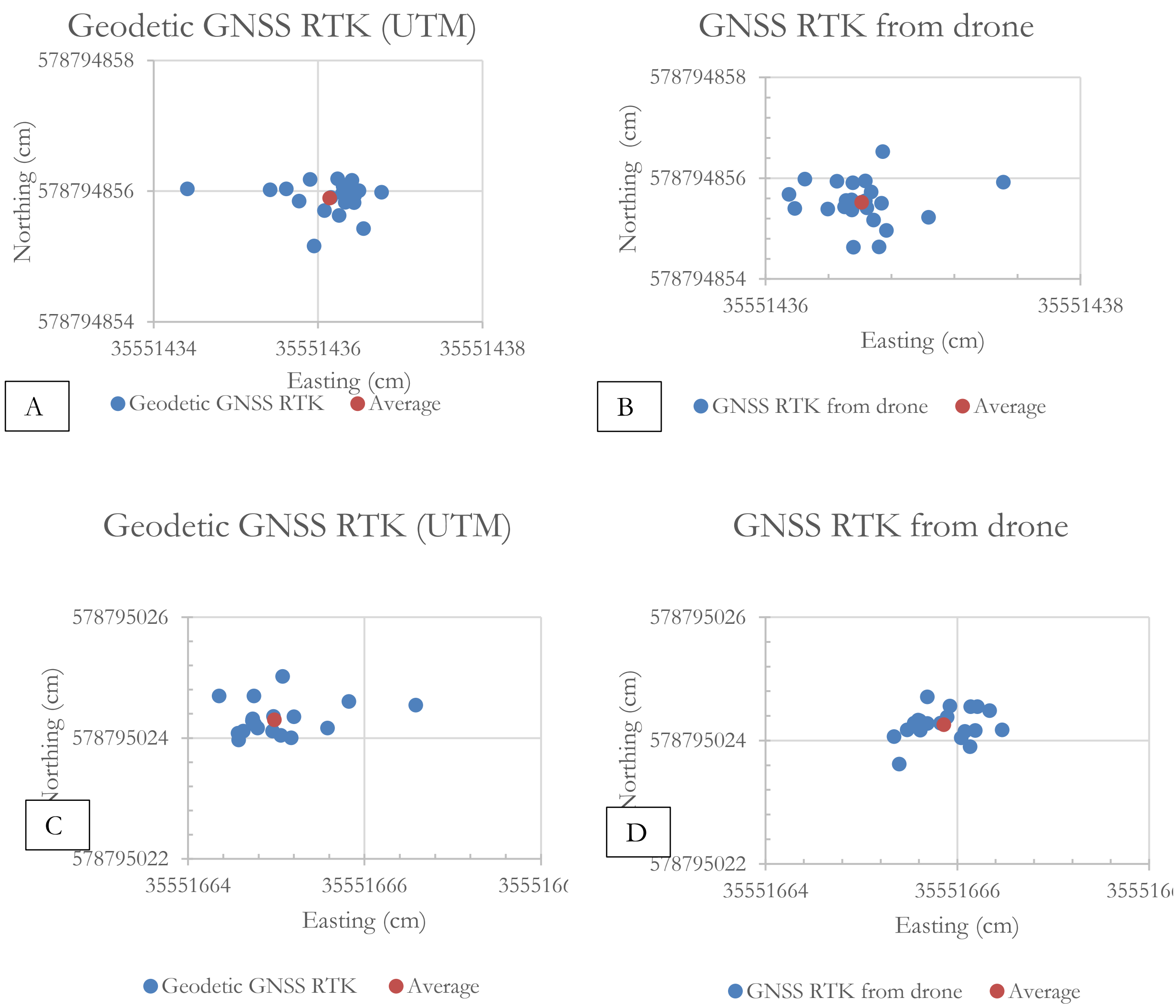

Figure 5-3: Figure 5-4: Graphical plot of the third experiment and their precision. A) Geodetic for location 1 B) Drone/UAV from location 1 C) Geodetic reading from location 2 D) Drone reading location 2

Table 5-3: Test results of the third experiment from location 1

Location 1	Easting (cm)	Northing (cm)	Height (cm)
Geodetic	35551436.139	578794855.895	8091.735
UAV	35551436.609	578794855.517	8091.447
Difference (Geodetic and UAV)	-0.47	0.37	0.287
STD	0.525857	0.593	0.854

Table 5-4: Test results of the third experiment from location 2

Location 2	Easting (cm)	Northing (cm)	Height (cm)
Geodetic	35551664.97	578795024.302	8089.47
UAV	35551665.8575	578795024.2585	8091.396
Difference (Geodetic and UAV)	-0.878	0.044	-1.92
STD	0.537628	0.39572982	1.79

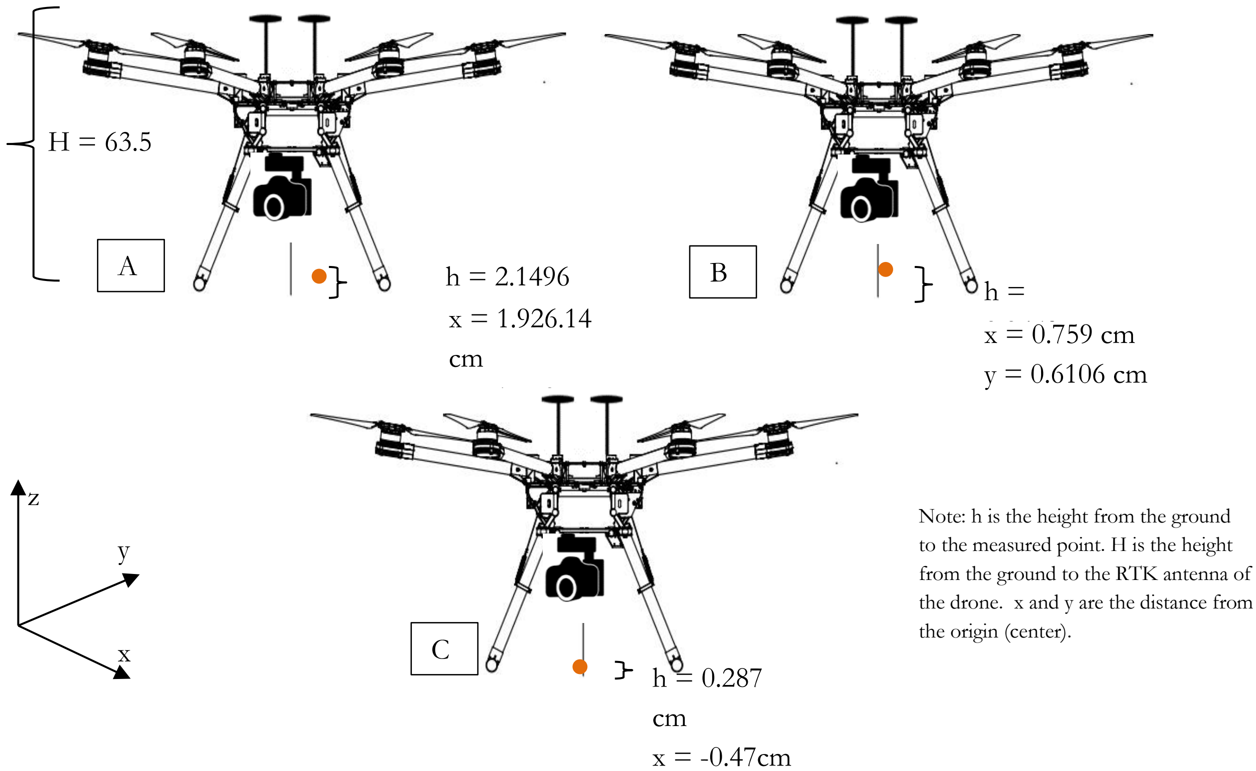

Figure 5-5: Illustration of GNSS RTK reference center for the three tests showing the difference between the geodetic GNSS (center) and the GNSS RTK from the drone A) Geodetic GNSS Reciever on top of the antenna pole B) Geodetic GNSS Reciever on top of the drone C) Geodetic GNSS Reciever on tripod for location 1. (Modified after DJI user manual Matrice 600 Pro, 2016)

In general, the three experiments conducted indicate that the horizontal component of the x- and y-axes reading from the GNSS RTK reading of the drone refers the point in the middle of the two RTK antenna as the difference is quite closer to the central point of the drone. The results of the height component show the location closer to the ground point, and hence the ground point (ground surface) is the point of reference for the RTK measurement of the drone. In other words, the reference point is 63.5 cm below the RTK antenna height of the drone. The measured height of the camera is 14 cm from the ground when it is in the nadir view and the height to the top of the gimbal (point k in Figure 4-6 and Figure 5-7) is 33.5 cm from the ground.

5.2. Test flight and data acquisition

The test is aimed at validating the capability of the aircraft and its GNSS RTK system for fast and accurate mapping purposes. The test flight was carried out in Bentelo in the western part of Enschede, The Netherlands (Figure 4-1 and Figure 5-6). GCPs were collected, and it had two purposes; the first was to use it for aerial triangulation and the second was to assess the spatial accuracy of direct georeferencing obtained from onboard GNSS RTK measurements. Easily recognizable 40x40 cm plastic markers were used for GCP's. The measurements were taken with a very accurate static Leica GNSS RTK. Eight GCP's were used in total for image processing. Three test flights were conducted. A total of 70x70 m area was used for image acquisition. The initial distance of the base station from the aircraft was around 10 m before take-off, and its coordinates were measured using Leica GNSS RTK and updated into the system through DJI assistant for absolute location measurement. The height of the drone was 40 m above the ground for all of the three flight experiments. The images were acquired from the camera through SD card and the UAV flight log was obtained from the new custom-made synchronization module developed by dronexpert.nl (see section 3.6).

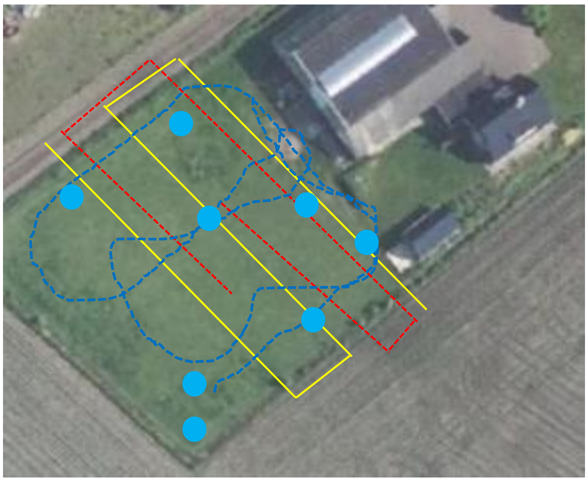

Figure 5-6: Flight trajectory and distribution of GCP for the three flights. Red dotted lines for the first flight; Blue doted irregular lines for second flights and solid yellow lines for the third flights.

Table 5-5: Flight parameters set for the test flight

Flight parameters	Values
Forward overlap	78%
Side Overlap	78%
GSD	1.33 cm/pixel
Flight height	40 m
Photoshoot interval of the camera	1 sec

5.3. Lever arm correction

The estimation of the lever arm offset between the GNSS and camera made use of the initial measurement of the physical distance between the points in the drone to systematically transform a point from the GNSS reference center to the final camera lens location (see Figure 4-6 and Figure 5-7). The measuring tape was used for rough estimation of distance measurements between the points. The distance for point k (i.e., 33.5 cm) is the distance from the ground to the top of the gimbal in Figure 5-7.

.

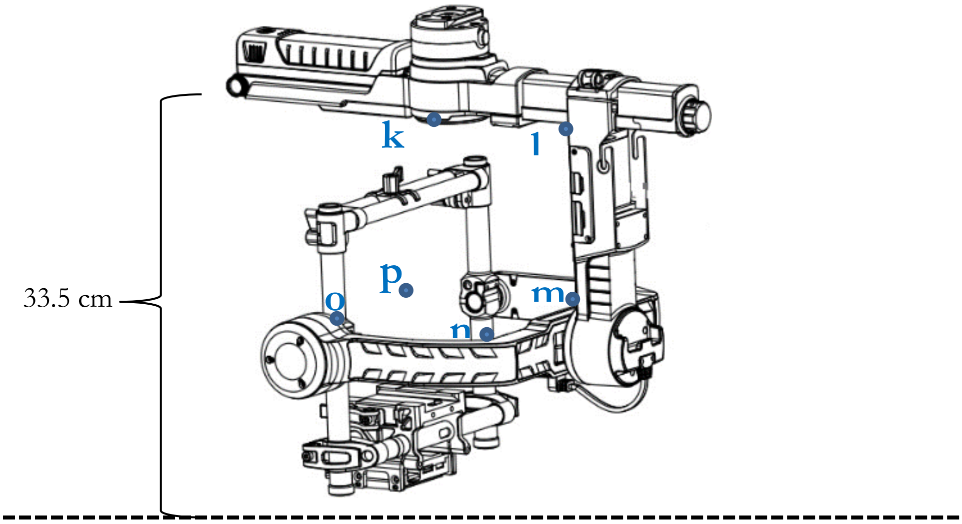

Figure 5-7: Translation vectors in the gimbal (from the top of the gimbal; point, k to the camera center point, p)

Table 5-6: Initially measured values for the offset estimation.

Distance between points	Points	Distance (cm)
Reference center (the ground) and point k	Tk	33.5
Point k and l	Tl	-11.5
Point l and m	Tm	-19.5
Point m and n	Tn	9
Point n and o	To	19
Point o and p	Tp	-12

5.3.1. GNSS RTK/Camera offset

Computation of the GNSS RTK/camera offset was done based on the initial measurements as an input value. The position information provided by the GNSS system of the drone was geographic coordinates which are defined by latitude and longitude in the geodetic system. The conversion of this coordinate system into the metric coordinate system was carried out since the values were given in degree. The conversion was done using Matlab code developed by Palacios, 2006. Using the developed methodology and procedure in section 4.4, estimation of the offset was done, and the result shows a variation of the lever arm with angles (Figure 5-8). The estimated values are highly dependent on the gimbal angles. The images were taken in nadir view, and the pitch angle was set in ~90^0, while the roll and yaw angle show high variation especially in the first flight (see Appendix 2). As it can be seen from the numbers labelled (the time the image was taken and its position and attituded data were recorded) in the Figure 5-8, the changes and the peak of the lever arm in the graph corresponds to the flight trajectory where there are changes in heading direction. The lever arm in the second flight in Figure 5-8 B is relatively constant compared to the other flights because it does not have sharp changes in the heading directions unlike the others. In other areas where there are no attitude changes, the lever arm is relatively constant in all of the three flights.

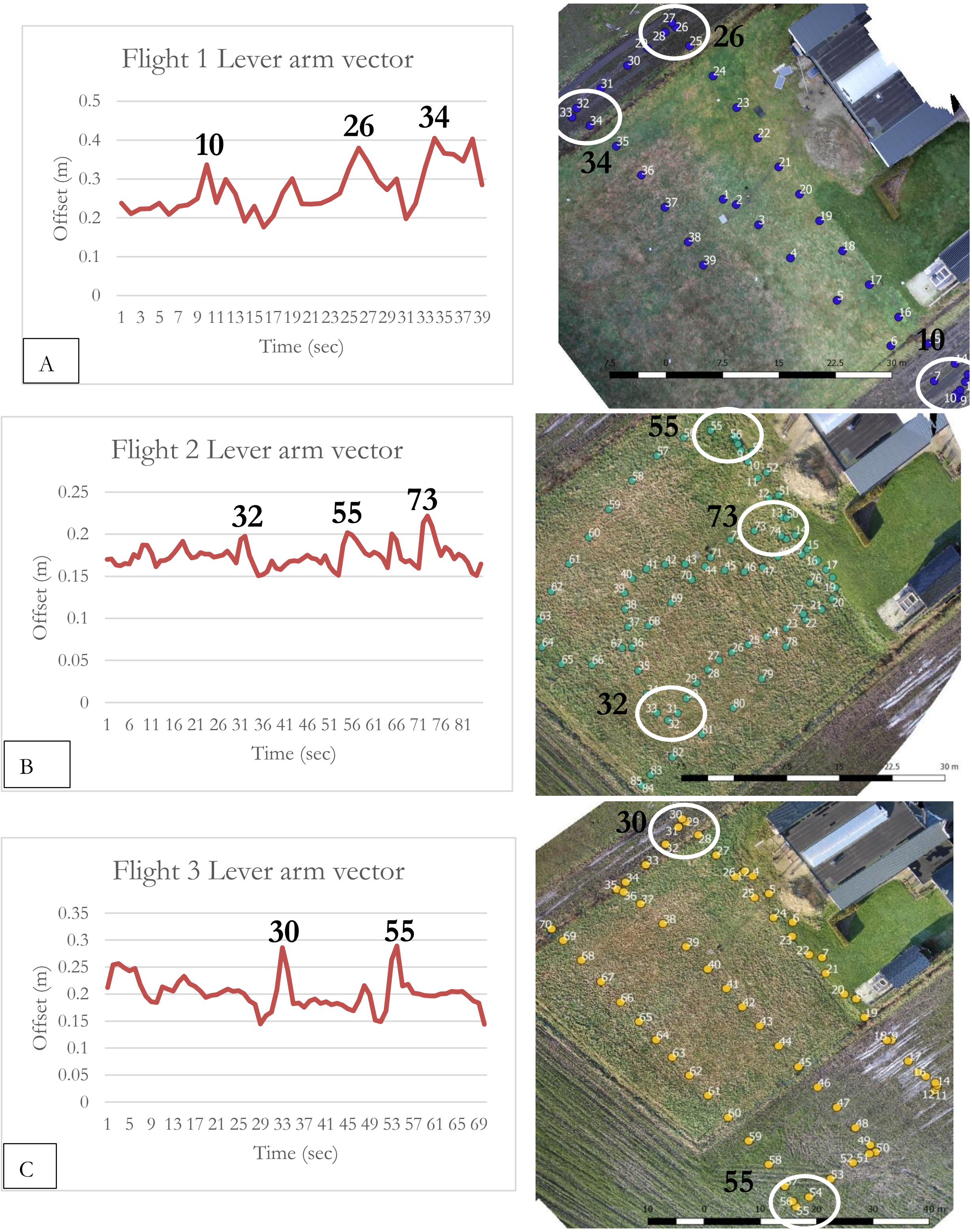

Figure 5-8: Lever arm offset between the GNSS reference center and camera lens with changes in attitude per images during the mission time for the three flights. A) the first flight B) the second flight and D) the third flight.

5.4. Assessing the results of direct georeferencing

The results of direct georeferencing were evaluated based on the computed value obtained from aerial triangulation. Aerial triangulation was performed in this study using the ground control points collected from the test area and performed in the Pix4D software package. The Pix4D project is completed automatically and contains three stages of processing; the initial phase; generation of dense point cloud and finally DSM and orthophoto generation.

5.4.1. Comparison of GNSS RTK with GCP assisted computed camera position

Camera position determined from photogrammetric bundle block adjustment (BBA) was compared and used as a reference point for camera position measurement directly from GNSS RTK unit onboard the aircraft. The calculated RMS errors for the three axes are shown on the BBA/RTK offset graph in Figure 5-9. It was noted that the angle measured by the gimbal reads incorrect value when the pitch angle exceeds 80 degrees in the first flight, and therefore temporary solution was used to put a plastic wedge on the gimbal (see Figure 5-10) for the second and third flight. The first flight was carried out by using automatic flight planning in Pix4D flight planning software. The time delay from the triggering module to the GNSS was set to 0.110 seconds for the first flight. This adjustment was made because the triggering module developed sends the triggering signal to the GNSS and the camera to take the data and the time the GNSS takes position data is faster than the time the camera captures the image. Therefore, the delay was introduced in the GNSS time so that it matches with the camera image capturing time. In general, RMSE calculated for the three axes is close to 1 m with x-axis having lower error recorded of 0.90 m (Figure 5-9) and the height component having RMSE of more than 1 meter.

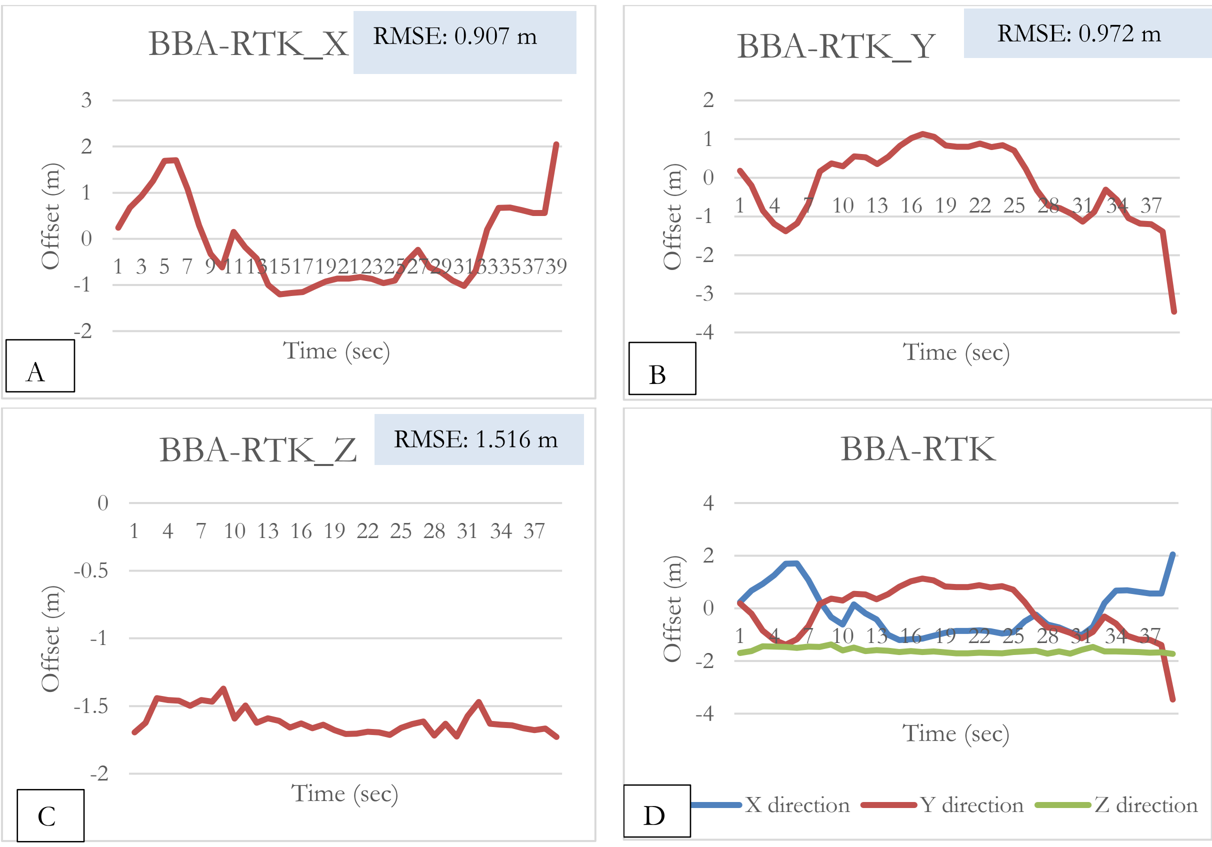

Figure 5-9: Comparison of BBA and GNSS RTK camera positions of the first flight for the; A) X-axis B) Y-axis C) Z axis and D) comparison of the three axes together. The RMSE is shown in the top right corner for every axis.

Since the gimbal angle measurement of the aircraft gives incorrect values when the gimbal pitch angle exceeds 80 degrees as mentioned above, in the second and third flight, manual adjustment of the gimbal has been made by placing plastic wedge (Figure 5-10) to keep the gimbal angle within a maximum value of 70 degree while the camera was still looking 90 degrees (nadir view) and the adjustment of 20 degrees has been made in the lever arm offset estimation to compensate for gimbal pitch angle. The manual flight was carried out in the second phase of the flight using flight controller, unlike the other flights. The time delay from the triggering module to the GNSS was set to 0.310 seconds in the second flight in order to better match the GNSS triggering time and the image capturing time as the higher displacement was observed during the first flight (Figure 5-9).

Figure 5-10: Gimbal set up and a plastic wedge placed to control pitch angle

From the total of 152 images, 85 images collected at the right flight height were selected for processing in the second flight. The results of GNSS RTK reading from the aircraft was then compared with the bundle adjusted camera position. The results of the difference (offsets) recorded are shown in Figure 5-11 for the three axes. The observed offsets alternate with different flight strips with the amplitude of 60 cm for the horizontal direction and a lower variation in the vertical direction of around 15 cm. The recorded offset is lower at the end of the flight strips due to the decrease in velocity as it will be discussed later in section 5.4.1.1. The RMS error of the offsets measured against the computed BBA position shows 0.32 m for x-axis and 0.395 m in the y-axis. The difference measured in the vertical component is 0.379 m.

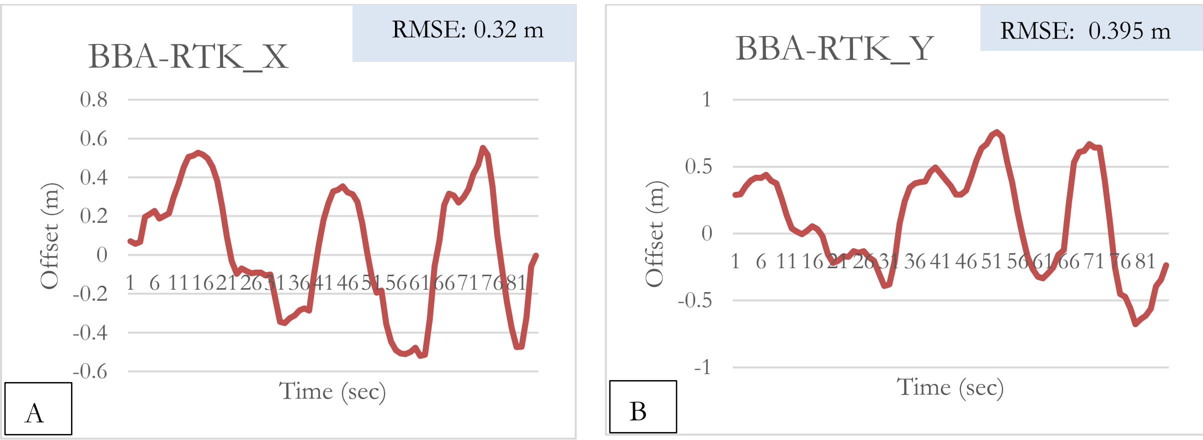

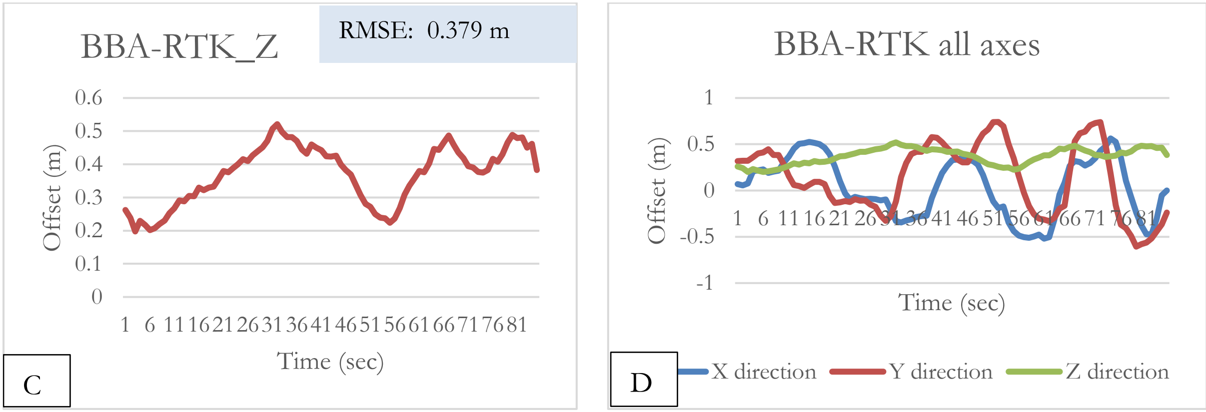

Figure 5-11: Comparison of BBA and GNSS RTK camera positions for the second flight. A) for X-axis B) Y-axis C) Z-axis D) for the three axes. The RMSE is shown in the top right corner for every axis.

The third flight was carried out using automatic flight planning Pix4D software. The time delay was set to 0.110 seconds the same as the first flight. The third flight used 70 images for processing. The observed offset shows that the initial part of the flight has a very large offset of up to 8 m and falls back to the lower offset variation. The large offset in the initial period of the flight is due to the mismatch between the GNSS triggering interval and the camera shooting interval. The GNSS is recorded twice or more in one second and skips in the next seconds while the camera is shooting continuously every second. The registered error of RMS in the horizontal component is 2.17 m, and the vertical direction is 0.1 m. The offset decreases significantly to 0.69 m in the horizontal directions and 0.08 m in the vertical directions when the first 11 readings are removed from the total of 70 images and GNSS readings that were processed.

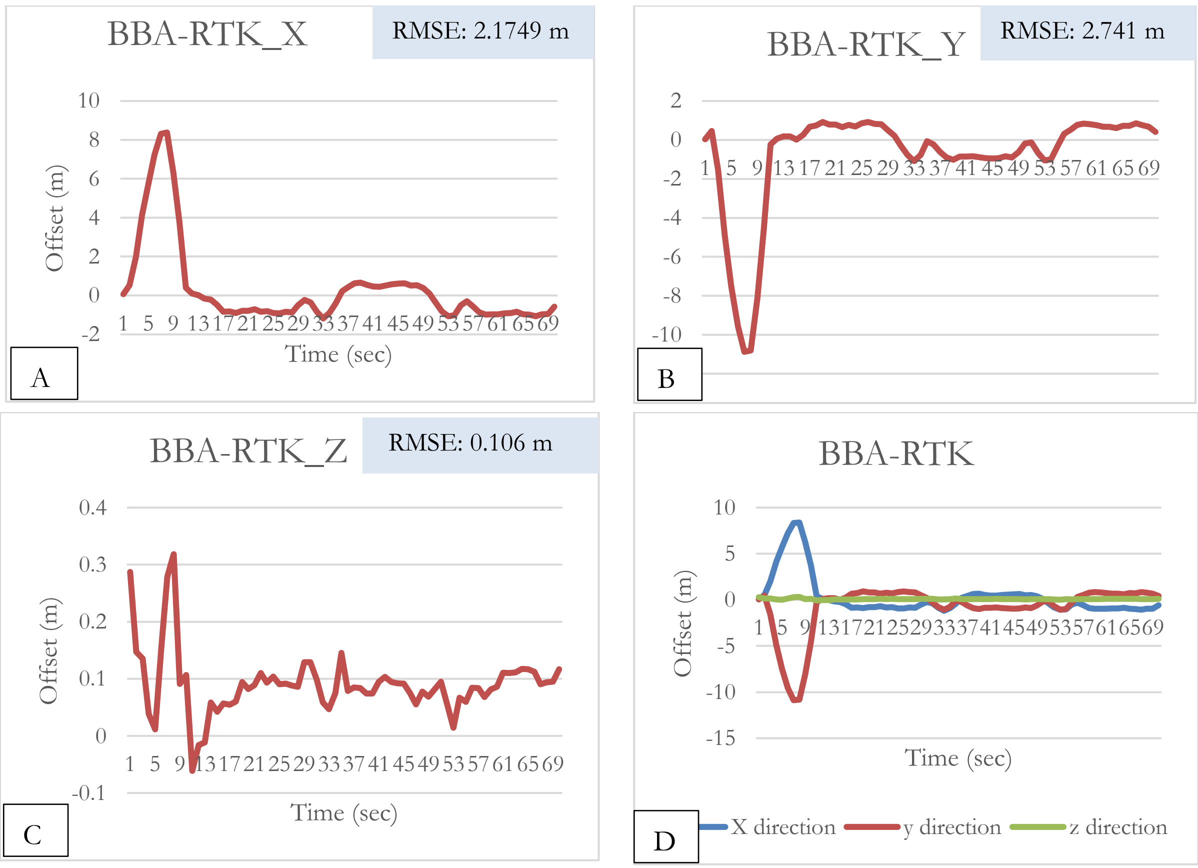

Figure 5-12: Comparison of BBA and GNSS RTK camera positions for the third flight. A) for X-axis B) Y-axis C) Z-axis D) for the three axes. The RMSE is shown in the top right corner for every axis.

The general comparison of the displacement (differences) observed for the three flights (Figure 5-13) show that the second flight has registered lower displacement errors measured against photogrammetrically adjusted projection centers when compared to the first and the third flights. The time adjustment and the manual flight plan contributed to the lower displacements in this case. The vertical displacement observed for the third flight is very small compared to its horizontal components because the mismatch of the GNSS and the camera time mentioned above for the first 11 readings affected the horizontal component and the vertical component remained an affected since the flight height was relatively constant. This means that mismatch of the position data and the image created the horizontal displacement while the flight height is relatively constant.

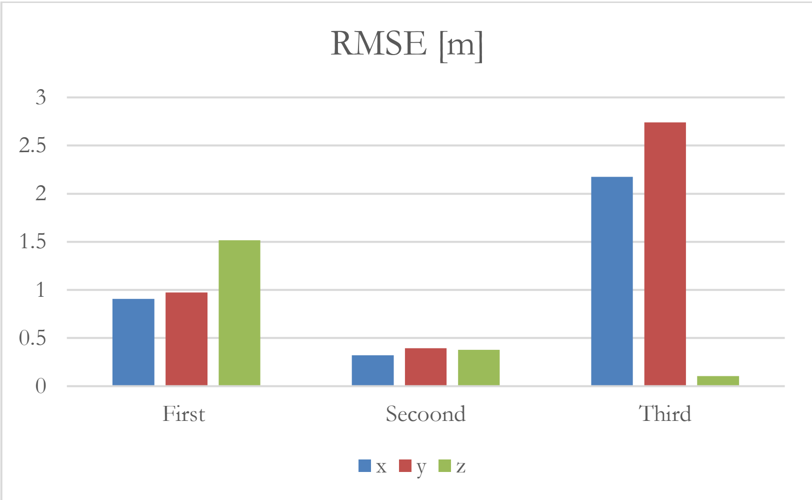

Figure 5-13: Comparison of the three flights for direct georeferencing

5.4.1.1. Aircraft speed and offset relation ship

The relation between the observed offset and speed of the aircraft is shown in Figure 5-14, Figure 5-16 and Figure 5-17. The magnitude of the error is highly related to the speed of aircraft. The higher the velocity of the aircraft, the higher offset or deviation from the assumed true values (BBA computed position in this case). In Figure 5-14 C, for the vertical component, the velocity of the aircraft is lower than the observed offset as the motion is more in the horizontal directions than it is in the vertical direction.

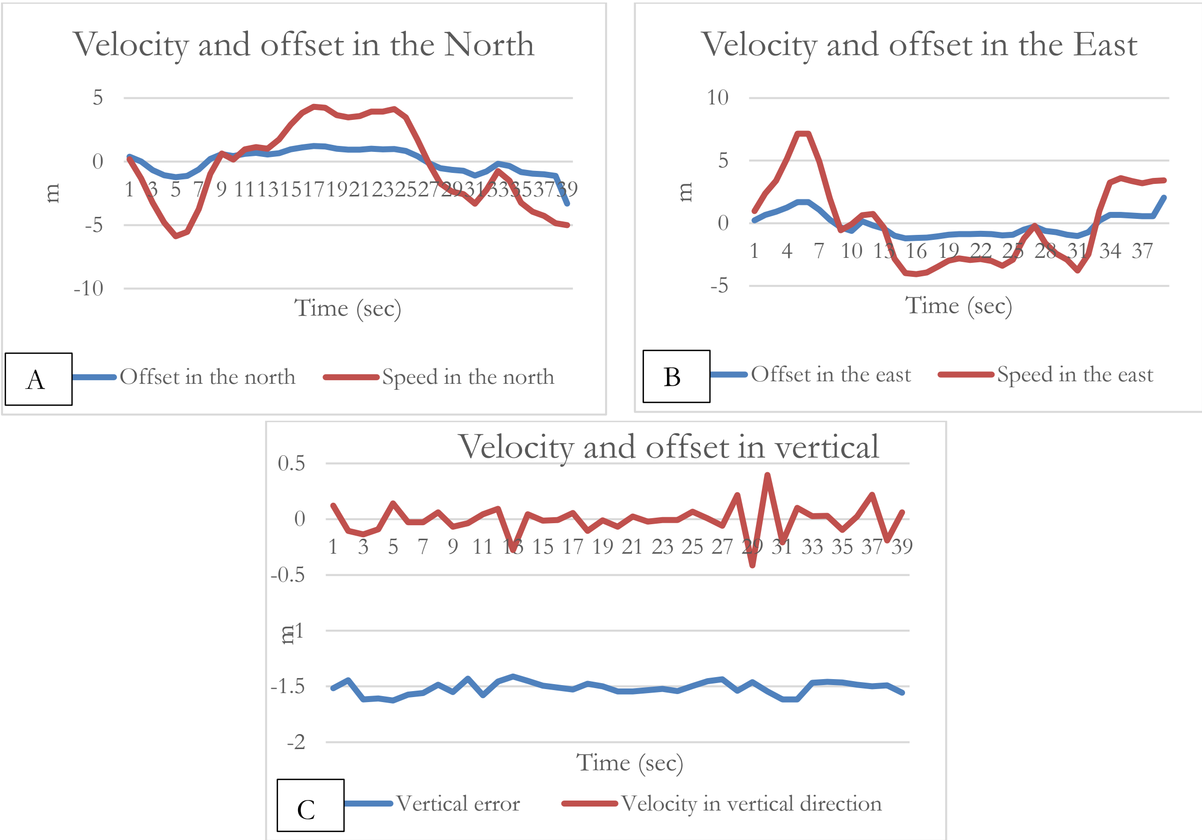

Figure 5-14: Positional error and velocity relation in the A) North B) East C) Vertical (Down) directions for the first flight

Positional measurements estimated through direct georeferencing and computed by indirect approach for the first flight are displayed on top of the generated orthophoto of the test area from the indirect approach in Figure 5-15. The arrows indicate the heading direction of the aircraft while in a mission. The yellow arrow shows the positive yaw direction, and the red arrow shows the negative reading direction of the heading values. The flight contains three major strips as can also be seen in Figure 5-15. The computed camera positions from bundle adjustment (Brown dots) are the accurate reference location of the camera positions. Location of the camera position measured directly from the GNSS RTK (white dots) and camera position after removing the effect of the lever arm (Blue dots) closer together. The three plots show a certain pattern in that the GCP assisted BBA locations show the camera positions ahead of the direct GNSS RTK measured camera locations in the flight direction (arrow pointing direction). The points in the central part of the flight zone (represented by a rectangle, A) are sparse and far apart when compared to areas on the bottom right part of the map (represented by a rectangle, B) indicating the velocity difference between the areas. The offset difference of horizontal distance is measured between points in QGIS software measurement tool. The measurement taken in the 12th second (rectangle B) and 19th second (rectangle A) were compared. Around 0.51 m offset is seen on the area marked by rectangle B and around 1 m is seen on the areas of rectangle A. The recorded velocity at the 12th second of the mission time was 1.36 m/s and 4.7 m/s at the 19th second of the mission time.

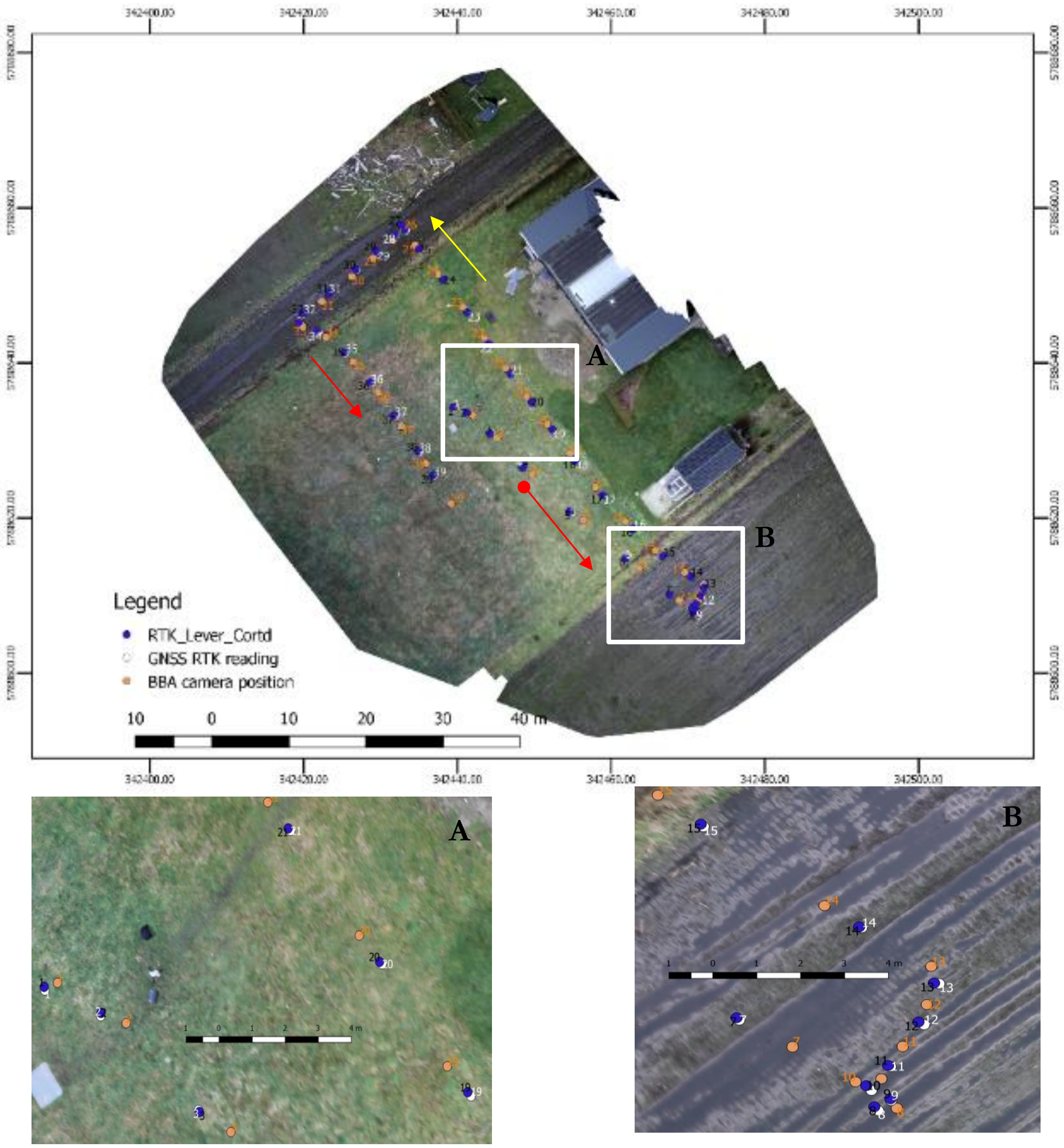

Figure 5-15: Comparison of camera position measured by direct georeferencing before (white)and after lever arm correction (blue) and those estimated by bundle block adjustment (brown)

Spatial plot of errors shows that there is a systematic error in the measurements. The plot of the points on the orthophoto shows a constant time delay. In the middle part of the image where the speed is higher around 4 m/s (the second and the last strip) measured around a mission time between 15 and 24 seconds, the recorded offset is 1.12 m. This shows that there is a time delay of about 0.28 second in this part of the trajectory. Therefore, there is a significant amount of time gap between the camera and GNSS affecting the accuracy of the direct georeferenced points. This can also be visible in the second and third flights (see Figure 5-16 and Figure 5-17). At the same aircraft speed of 4 m/s, the average offset observed for the second flight is 0.3 m and a time gap of 0.075 second can be estimated from the observed speed and offset.

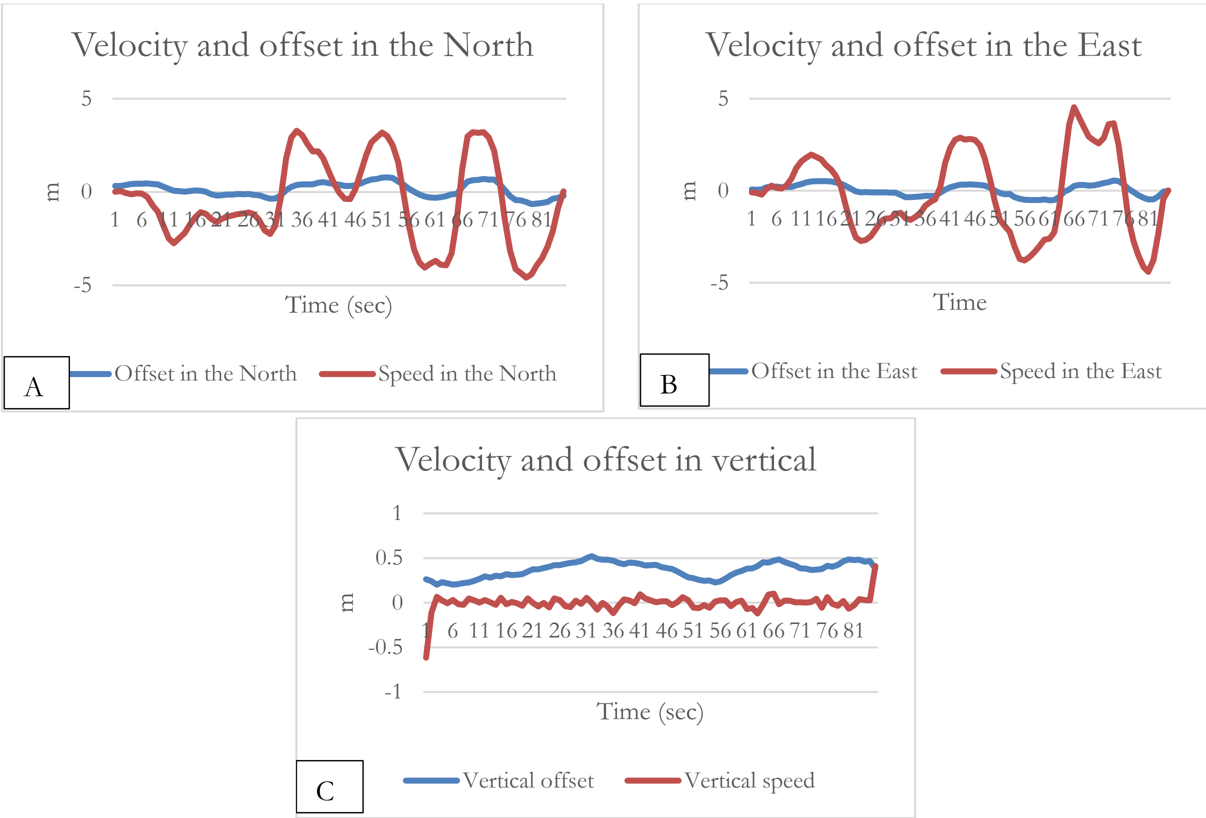

Figure 5-16: Positional error and velocity relation in the A) North B) East C) Vertical (Down) directions for the second flight

The large differences observed in the third flight for the first 11 readings have no association with the speed of the aircraft as it can also be seen from Figure 5-17. At the speed of 4 m/s in the horizontal direction, the measured offset of 0.7 m is observed and a time delay of 0.17 second can be estimated.

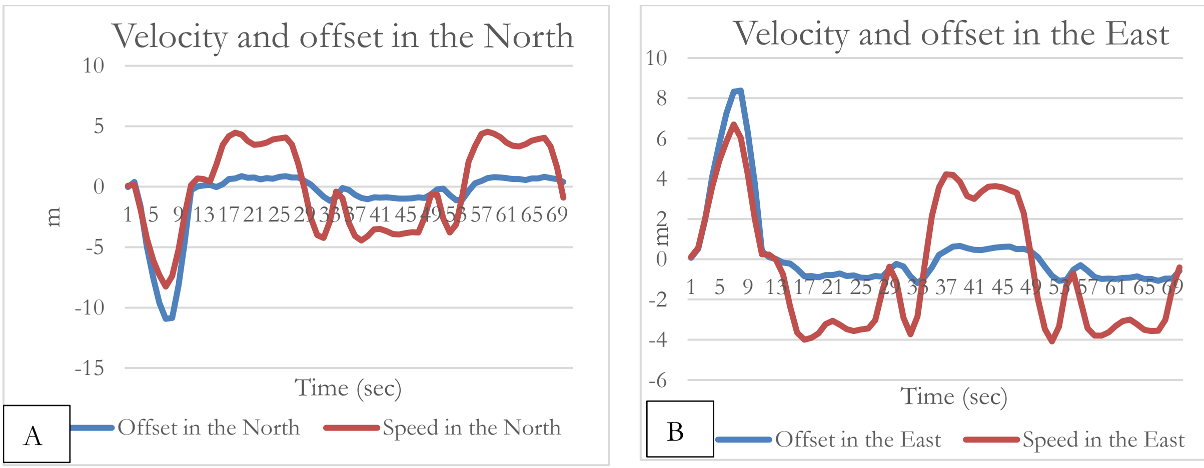

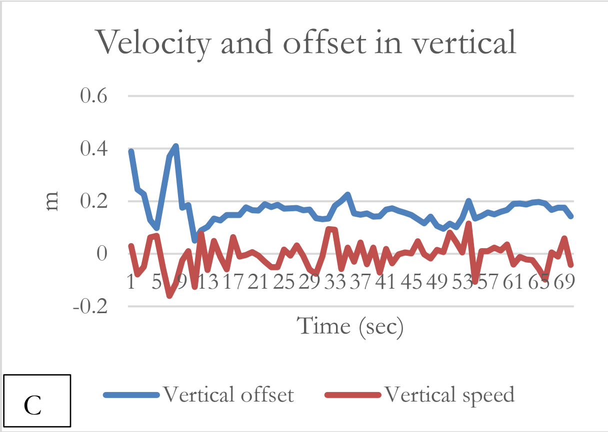

Figure 5-17: Positional error and velocity relation in the A) North B) East C) Vertical (Down) directions for the third flight

5.4.2. Geometric accuracy assessment based on control points

The accuracy of UAV image block orientation for direct georeferencing and indirect georeferencing was assessed using the ground control points and the check points evenly distributed in the study area for the flight experiments. The RMSE for the indirect georeferencing at GCP and CP points show a very low spatial error for image block orientation. The summary of spatial error at GCP's of the first flight for indirect georeferencing presented in Table 5-7 show RMSE of 2.5 cm in planimetric and a closer RMSE of 2.4 cm in the vertical direction. On the check points, the obtained accuracy is 2.7 cm in the planimetric and 8.7 cm in the height component. The spatial error of the first flight obtained for the direct georeferencing from RTK reading measured at check points is 33.6 cm in the horizontal and 40.8 cm in the vertical direction (Table 5-8).

Table 5-7: Summary of spatial error in indirect georeferencing for the first flight data set

Type	No.		XY Error[m]	Z Error[m]
GCP	4	Mean	-0.002	-0.011
		Sigma	0.025	0.022
		RMSE	0.025	0.024
Check points	2	Mean	-0.006	-0.055
		Sigma	0.015	0.067
		RMSE	0.027	0.087

Table 5-8: Summary of spatial error in direct georeferencing for the first flight data set

Type	No.		XY Error[m]	Z Error[m]
Check points	4	Mean	-0.07	-0.4
		Sigma	0.273	0.0812
		RMSE	0.336	0.408

The second flight data set shows improved accuracy for both direct and indirect georeferencing results (Table 5-9). The RMSE measured for the indirect approach at GCP is 0.6 cm and 3.9 cm for the planimetric and height components respectively. The spatial RMSE at check points obtained show 1.3 cm in the planimetric and 16 cm in the height component. The residual error registered at check points for direct georeferencing using RTK solution is 31 cm in the planimetric and 27.2 cm for the height direction (Table 5-10).

Table 5-9: Summary of spatial error in indirect georeferencing for the second flight data set

Type	No.		XY Error[m]	Z Error[m]
GCP	5	Mean	-0.00004	0.010
		Sigma	0.006	0.037
		RMSE	0.006	0.039
Check points	3	Mean	-0.009	0.098
		Sigma	0.008	0.125
		RMSE	0.013	0.16

Table 5-10: Summary of spatial error in direct georeferencing for the second flight data set

Type	No.		XY Error[m]	Z Error[m]
Check points	8	Mean	-0.11	-0.264
		Sigma	0.266	0.064
		RMSE	0.31	0.272

The residual error measured at the GCP location for the third flight is 1 cm for the horizontal direction and 1.9 cm in the vertical direction for the indirect georeferencing (Table 5-11). On the check points, the obtained accuracy is 1.6 cm for the planimetric measurement and 0.8 cm for the height component. The quality of direct georeferencing measured against the check points show an RMSE of 58.2 cm in the planimetric and 56.3 cm in the height component (Table 5-12).

Table 5-11: Summary of spatial error in indirect georeferencing for the third flight data set

Type	No.		XY Error[m]	Z Error[m]
GCP	5	Mean	0.0007	-0.000304
		Sigma	0.01	0.019
		RMSE	0.01	0.019
Check points	3	Mean	-0.004	0.003
		Sigma	0.011	0.007
		RMSE	0.016	0.008

Table 5-12: Summary of spatial error in direct georeferencing for the third flight data set

Type	No.		XY Error[m]	Z Error[m]
Check points	8	Mean	-0.159	-0.562
		Sigma	0.423	0.0262
		RMSE	0.582	0.563

The comparison of spatial error of the three flights is shown in Figure 5-18 for image block orientation from direct georeferencing. The horizontal and vertical component measured at the check points for the three flights show that the second test flight carried out manually outperformed the first and the third flights because of the time delay adjustment made in the triggering module. In addition to that, the automatic flight planning has a problem of updating RTK way points because of the DJI bug which affects the quality of the end product.

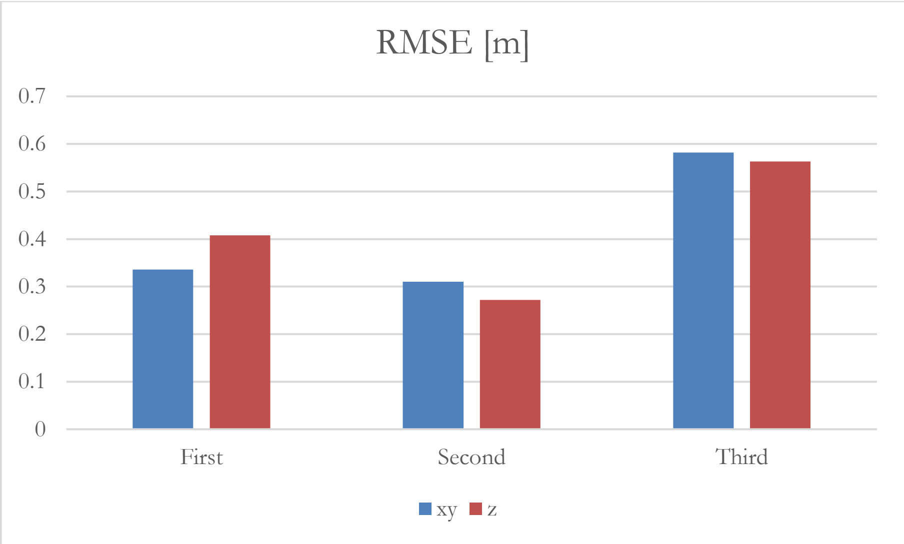

Figure 5-18: Comparison of geometric RMSE for the three flights of direct georeferencing assessed against check points.

5.5. Implication of obtained direct georeferencing result for natural hazard application

Standard photogrammetry has limited applications when it comes to natural hazard areas such as snow, avalanches, landslides requiring rapid responses because of the difficulties in placing the GCPs and the time needed to process the images. Direct georeferencing can provide the required images and location information at a much faster speed. The direct georeferencing result in this study can be used in two ways, the first is to use the image from the aircraft directly with GNSS RTK information and the second is to process the images to obtain orthophoto for wider coverage of the area. The first is faster especially when an immediate response is needed after disaster for rescue operations and the second could be used for post-disaster assessment of the area. The decimetre accuracy obtained for direct georeferencing from GNSS RTK reading in this study ranging between 30 cm to 1 m can be a good solution for both approaches. The results are quite sufficient to use it for disaster management purposes based on the spatial distance of features on the ground (i.e., people, building, roads). The products can also be integrated with GIS databases and can be used to create hazard maps. The simulation of the process of image acquisition and disaster response is shown in Figure 5-19 in which Matrice 600 Pro is used for image acquisition from the area affected by natural hazard and orthophoto generated from the acquired images is used as an information source for rescue operators. Figure 5-20 shows the process of post-disaster damage assessment in which the high-resolution orthophoto is used for damage assessment. The comparison with google earth image shows that with the same resolution (zooming scale), google earth image is highly blurred to identify and grade the damage scale and this is true especially in the areas where high-resolution google images are not available. The generated orthoimage, on the other hand, shows the roof of the building very clearly, and hence it is possible to scale the damage with some level of confidence. In general, the drone used for this study has multiple significance for natural hazard areas because of its wide coverage relative to other multirotor UAVs and its ability to host more than one sensor at the same time. It can be used for collecting thermal images by installing thermal sensors in areas of fire damages, and other building damage assessment works. Multispectral images can also be acquired by using multispectral cameras in the drone.

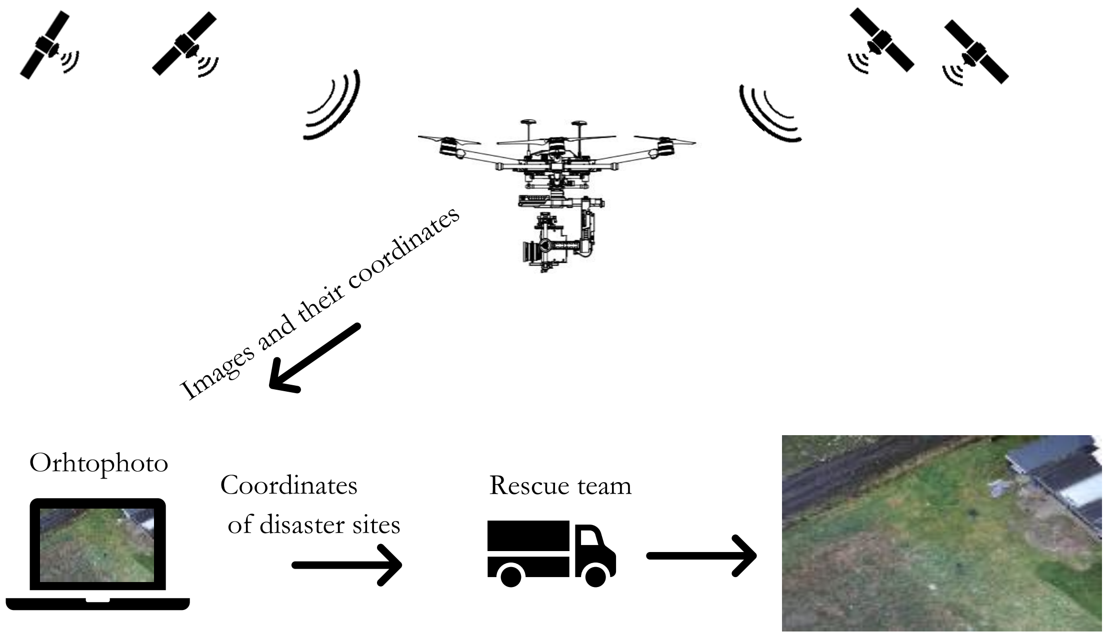

Figure 5-19: Simulation of disaster response using generated orthophoto

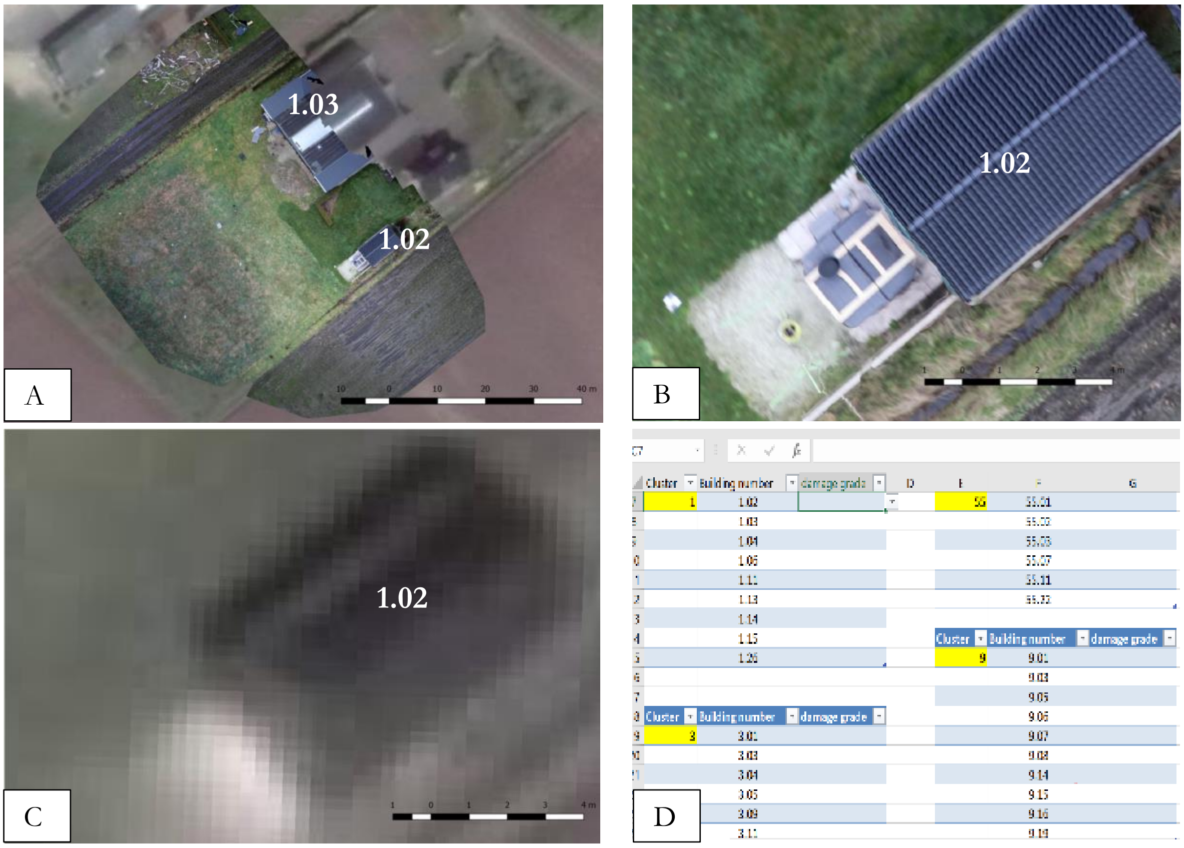

Figure 5-20: Example of how the generated Orthophoto can be used for post-disaster damage assessment and its advantage over google earth image for this case (i.e., rural areas) A) Orthophoto overlaid on google earth image B) Enlarged view of building number 1.02 in A, C) Enlarged view of the same building from google earth image D) Damage assessment scale

6. CONCLUSION AND RECOMMENDATION

6.1. Conclusion

The main goal of this study was to assess the quality of GNSS RTK on Matrice 600 Pro for direct georeferencing. In order to do that the GNSS RTK reference center and GNSS RTK/camera offset had to be determined (sub-objectives). The three experiments carried out to determine the GNSS RTK reference center of the Matrice 600 Pro indicated that the ground surface (where the drone stands) is the reference center for the RTK measurements of the drone. In other words, the positional reading from RTK is approximately 63.5 cm (the height of the RTK antenna from the ground) below the phase center of the RTK antenna on the drone. The camera is found 14 cm above the ground (i.e., reference center) in the vertical direction when it is in the nadir view. Implementation of the process of direct georeferencing required the correction factor for this GNSS RTK/camera offset also referred in this study as lever arm offset in all of the three axes which might cause higher displacement when projected onto the ground. The lever arm was computed based on the initial measurement made manually using measuring tape. The lever arm offset plotted for the three axes show a strong relation with rotation angles of the aircraft, and it varies as the aircraft and its gimbal angle changes. Hence it is possible to say that the lever arm offset is dependent on the attitude angle. The quality of the direct georeferencing obtained in the second flight shows a relatively higher accuracy for both direct comparisons with BBA position and image block orientation accuracy in the horizontal component. The results of direct georeferencing described in section 5.4.1 of direct comparison with GCP assisted BBA position and direct georeferencing assessed against check points described in section 5.4.2 show that geometric accuracy of the direct georeferencing increases when photogrammetric adjustment is used. This also means that the direct georeferencing with GNSS RTK onboard can generate a point cloud with decimetre accuracy good enough for mapping purposes. The overall behavior of the error pattern observed for direct georeferencing indicated that there is a systematic error between measured points. A time delay of 0.17 second was observed from the offset of 67 cm at aircraft velocity of 4 m/s in the first flight and with the same speed of 4 m/s, a time delay of 0.075 seconds was registered in the second data set from the average offset of 30 cm. The highest peak (in the absolute term) in the BBA and GNSS RTK graph of spatial offset matches with highest velocity and time delay. The observed relationship between the speed of the aircraft and the recorded offset revealed that the time delay between the GNSS and the camera was the reason for the higher errors observed in direct georeferencing. From this, it is possible to conclude that the synchronization error played a greater role in the recorded low accuracy of the direct georeferencing result. From the three flights carried out using manual and automated flight planning, the manual flights performed better in providing good accuracy. The automated flights seem to have difficulties in accurately updating the waypoints as it was in the third flight. In general, the GNSS RTK on the drone provides a very accurate result because the first experiment carried out to determine the reference center showed high accuracy with reference to the geodetic GNSS RTK measurements. However, the time synchronization between the GNSS and the camera was not accurate which resulted in low accuracy for direct georeferenced products. In addition to that, the lever arm offset estimation depends on the accuracy of the manual measurements made for initial estimation and hence the total obtained accuracy depends on the accuracy of lever arm offset determined. Based on the spatial distance of ground features (i.e., people, buildings, etc.), the overall achieved result for direct georeferencing is quite sufficient for natural hazard applications especially those requiring rapid responses such as rescue missions as well as post-disaster damage assessment.

6.2. Recommendation

The objectives of this research have been met with the data and information collected during the study. However, due to the limitation of time, this research was done in a smaller area, and the boresight angle estimation and its effects were not conducted. Therefore, based on this, the further recommendation is given on the following:

- Detail analysis of the capability of the GNSS RTK on Matrice 600 Pro covering the wider area to evaluate the distance covered and the quality of the GNSS measurement.
- Analysis of Boresight misalignment on direct georeferencing and its effects on the resulting photogrammetric product.

LIST OF REFERENCES

Al-Shaery, A., Zhang, S., & Rizos, C. (2013). An enhanced calibration method of GLONASS inter-channel bias for GNSS RTK. *GPS Solutions*, *17*(2), 165–173. https://doi.org/10.1007/s10291-012-0269-5

Bäumker, M., & Heímes, F. J. (2001). New calibration and computing method for direct georeferencing of image and scanner data using the position and angular data of an hybrid inertial navigation system. *OEEPE Workshop*, 1–17. Retrieved from https://s3.amazonaws.com/mics.pix4d.com/KB/documents/baheimesoeepe.pdf

Blanco, J. (2014). *A tutorial on se (3) transformation parameterizations and on-manifold optimization*. *University of Malaga, Tech. Rep.* Retrieved from http://sites.google.com/site/jlblancosite/

Bryson, M., & Sukkarieh, S. (2015). *UAV localization using inertial sensors and satellite positioning systems*. *Handbook of Unmanned Aerial Vehicles*. https://doi.org/10.1007/978-90-481-9707-1

Chapala, S. R., Pirati, G. S., & Nelakuditi, U. R. (2016). Determination of coordinate transformations in UAVS. In *Proceedings - 2016 2nd International Conference on Cognitive Computing and Information Processing, CCIP 2016*. https://doi.org/10.1109/CCIP.2016.7802861

Chiang, K. W., Tsai, M. L., & Chu, C. H. (2012). The development of an UAV borne direct georeferenced photogrammetric platform for ground control point free applications. *Sensors (Switzerland)*, *12*(7), 9161–9180. https://doi.org/10.3390/s120709161

Cramer, M., Stallmann, D., & Haala, N. (2000). Direct georeferencing using GPS/inertial exterior orientations for photogrammetric applications. *International Archives of Photogrammetry and Remote Sensing*, *33*(B3), 198–205. https://doi.org/10.1017/CBO9780511777684

DJI user manual Datalink Pro. (2016). *Datalink pro*. Retrieved from www.dji.com/product/datalink-pro

DJI user manual Matrice 600 Pro. (2016). *MATRICE 600 PRO*. Retrieved from https://dl.djicdn.com/downloads/m600/20170717/Matrice_600_User_Manual_v1.0_EN.pdf

DJI user manual Ronin-MX. (2016). *RONIN-MX User Manual*. Retrieved from https://dl.djicdn.com/downloads/ronin-mx/en/Ronin-MX_User_Manual_V1.2_en_20160711.pdf

Eisenbeiss, H. (2004). A mini Unmanned Aerial Vehical (UAV): System overview and image acquisition. *International Archives of Photogrammetry, Remote Sensing and Spatial Information Sciences*, *XXXVI*(5/W1).

Eisenbeiß, H., Zurich, E. T. H., Eisenbeiß, H., & Zürich, E. T. H. (2009). *UAV photogrammetry*. *Institute of Photogrammetry and Remote Sensing*. University of Technology Dresden. https://doi.org/doi:10.3929/ethz-a-005939264

Gerke, M., & Przybilla, H.-J. (2016). Accuracy analysis of photogrammetric UAV image blocks: Influence of onboard RTK- GNSS and cross flight patterns. *Photogrammetrie - Fernerkundung - Geoinformation*, *2016*(1), 17–30. https://doi.org/10.1127/pfg/2016/0284

Gómez-Candón, D., De Castro, A. I., & López-Granados, F. (2014). Assessing the accuracy of mosaics from unmanned aerial vehicle (UAV) imagery for precision agriculture purposes in wheat. *Precision Agriculture*, *15*(1), 44–56. https://doi.org/10.1007/s11119-013-9335-4

Hofmann-Wellenhof, B., Lichtenegger, H., & Wasle, E. (2008a). *GNSS – Global Navigation Satellite Systems - GPS, GLONASS, Galileo, and more*. *Applied Sciences*. SpringerWienNewYork. https://doi.org/10.1007/978-3-211-73017-1

Hofmann-Wellenhof, B., Lichtenegger, H., & Wasle, E. (2008b). *GNSS — Global Navigation Satellite Systems*. https://doi.org/10.1007/978-3-211-73017-1

Hutton, J., Lipa, G., & Lutes, J. (2014). White Paper DMS-UAV Accuracy Assessment : AP20 with Nikon D800E White Paper, 1–6. Retrieved from https://www.applanix.com/?articleattachment=20

Ip, A., Mostafa, M., Hutton, J., & Barriere, J. (2008). An optimally integrated direct georeferencing and flight management system for increased productivity of airborne mapping and remote sensing. *Remote Sensing and Spatial Information Sciences*, *XXXVII*(Part B1), 579–584. Retrieved from http://www.isprs.org/proceedings/XXXVII/congress/1_pdf/98.pdf

Ip, A. W. L. (2005). *Analysis of integrated sensor orientation for aerial mapping*. Retrieved from http://www.geomatics.ucalgary.ca/links/GradTheses.html

Jacobsen, K. (2002). Calibration aspects in direct georeferencing of frame imagery. *International Archives of Photogrammetry Remote Sensing and Spatial Information Sciences*, *34*, 82–88. Retrieved from http://www.isprs.org/proceedings/XXXIV/part1/paper/00013.pdf

Kouba, J. (2009). A Guide to using international GNSS Service (IGS) Products. *Geodetic Survey Division Natural Resources Canada Ottawa*, *6*, 34. Retrieved from https://www.researchgate.net/profile/Jan_Kouba/publication/228663800_A_guide_to_using_International_GNSS_Service_IGS_products/links/54fcc30c0cf270426d102cd3.pdf

Liba, N. and, & Berg-Jürgens, J. (2015). Accuracy of orthomosaic generated by different methods in example of UAV platform MUST Q. *IOP Conference Series: Materials Science and Engineering*, *96*(1), 12041. https://doi.org/10.1088/1757-899X/96/1/012041

Lo, C. F., Tsai, M. L., Chiang, K. W., Chu, C. H., Tsai, G. J., Cheng, C. K., … Ayman, H. (2015). The Direct Georeferencing application and performance analysis of UAV helicopter in GCP-free area. *International Archives of the Photogrammetry, Remote Sensing and Spatial Information Sciences - ISPRS Archives*, *40*(1W4), 151–157. https://doi.org/10.5194/isprsarchives-XL-1-W4-151-2015

Mian, O., Lutes, J., Lipa, G., Hutton, J. J., Gavelle, E., & Borghini, S. (2015). Direct georeferencing on small unmanned aerial platforms for improved reliability and accuracy of mapping without the need for ground control points. In *International Archives of the Photogrammetry, Remote Sensing and Spatial Information Sciences - ISPRS Archives* (Vol. 40, pp. 397–402). https://doi.org/10.5194/isprsarchives-XL-1-W4-397-2015

Morales, Y., & Tsubouchi, T. (2007). DGPS, RTK-GPS and StarFire DGPS performance under tree shading environments. In *IEEE ICIT 2007 - 2007 IEEE International Conference on Integration Technology* (pp. 519–524). https://doi.org/10.1109/ICITECHNOLOGY.2007.4290370

Mostafa, M. M. R., & Hutton, J. (2001). Direct positioning and orientation systems. How do they work ? What is the attainable accuracy. In *Proceedings, American Society of Photogrammetry and Remote Sensing Annual Meeting*. Retrieved from http://www.simwright.com/techpapers/POS-AV/POS AV_2_Direct Positioning.pdf

Odijk, D., Zhang, B., & Teunissen, P. J. G. (2015). Multi-GNSS PPP and PPP-RTK: Some GPS+BDS results in Australia. In *Lecture Notes in Electrical Engineering* (Vol. 341, pp. 613–623). Springer, Berlin, Heidelberg. https://doi.org/10.1007/978-3-662-46635-3_52

Pfeifer, N., Glira, P., & Briese, C. (2012). Direct georeferencing with on board navigation components of light weight UAV platforms. *International Archives of the Photogrammetry, Remote Sensing and Spatial Information Sciences - ISPRS Archives*, *39*(September), 487–492. https://doi.org/10.5194/isprsarchives-XXXIX-B7-487-2012

Rafael Palacios. (2006). deg2utm - File Exchange - MATLAB Central. Retrieved February 12, 2018, from https://nl.mathworks.com/matlabcentral/fileexchange/10915-deg2utm

Rehak, M., Mabillard, R., & Skaloud, J. (2013). A Micro-UAV with the capability of direct georeferencing. *International Archives of Photogrammetry and Remote Sensing, Beijing, China*, *XL*(September), 4–6. https://doi.org/10.5194/isprsarchives-XL-1-W2-317-2013

Rehak, M., & Skaloud, J. (2017). Time synchronization of consumer cameras on Micro Aerial Vehicles. *ISPRS Journal of Photogrammetry and Remote Sensing*, *123*, 114–123. https://doi.org/10.1016/j.isprsjprs.2016.11.009

Rost, C., & Wanninger, L. (2009). Carrier phase multipath mitigation based on GNSS signal quality measurements. *Journal of Applied Geodesy*, *3*(2), 1–8. https://doi.org/10.1515/JAG.2009.009

Ruzgiene, B., Berte, T., Ge, S., Jakubauskiene, E., & Aksamitauskas, V. C. (2015). The surface modelling based on UAV Photogrammetry and qualitative estimation. *Measurement: Journal of the International Measurement Confederation*, *73*, 619–627. https://doi.org/10.1016/j.measurement.2015.04.018

Skaloud, J. (1999). Problems in Direct-Georeferencing by INS/DGPS in the airborne environment. *Invited Paper, ISPRS Workshop on 'Direct versus*, 1–9. Retrieved from https://pdfs.semanticscholar.org/baa0/7d70f97afbd18307e5310d566bf89da65b1b.pdf

Souza, E. M. de, Monico, J. F. G., & Pagamisse, A. (2009). GPS satellite kinematic relative positioning: Analyzing and improving the functional mathematical model using wavelets. *Mathematical Problems in Engineering*, *2009*, 1–18. https://doi.org/10.1155/2009/934524

Spockeli, B. A. (2015). *Integration of RTK GPS and IMU for Accurate UAV Positioning*. Norwegian University of Science and Technology. Retrieved from https://brage.bibsys.no/xmlui/handle/11250/2352452

Turner, D., Lucieer, A., & Wallace, L. (2014). Direct georeferencing of ultrahigh-resolution UAV imagery. *IEEE Transactions on Geoscience and Remote Sensing*, *52*(5), 2738–2745. https://doi.org/10.1109/TGRS.2013.2265295

Walpersdorf, A., Bouin, M. N., Bock, O., & Doerflinger, E. (2007). Assessment of GPS data for meteorological applications over Africa: Study of error sources and analysis of positioning accuracy. *Journal of Atmospheric and Solar-Terrestrial Physics*, *69*(12), 1312–1330. https://doi.org/10.1016/j.jastp.2007.04.008

Xu, H. (2012). Application of GPS-RTK technology in the land change survey. *Procedia Engineering*, *29*, 3454–3459. https://doi.org/10.1016/j.proeng.2012.01.511

Zhang, W., Ghogho, M., & Yuan, B. (2012). Mathematical model and matlab simulation of strapdown inertial navigation system. *Modelling and Simulation in Engineering*, *2012*. https://doi.org/10.1155/2012/264537

APPENDIX

Appendix 1: Quaternion to Euler angle conversion formula (Blanco, 2014):

$$\phi = tan^{-1}(2\frac{q_r q_z + q_x q_y}{1-2(q_y^2+q_z^2)}$$
$$x = sin^{-1}(2(q_r q_y - q_x q_z))$$
$$\psi = tan^{-1}(2\frac{q_r q_x + q_y q_z}{1-2(q_x^2+q_y^2)}$$

Appendix 2: Platform dynamics

Flight 1

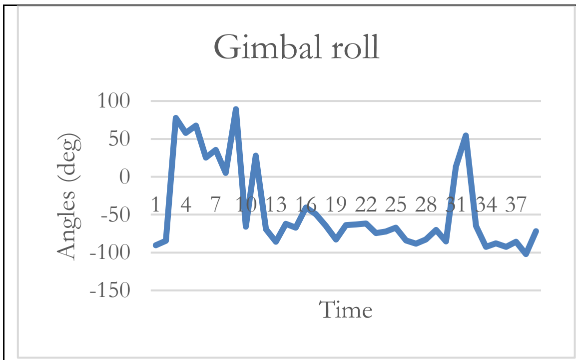

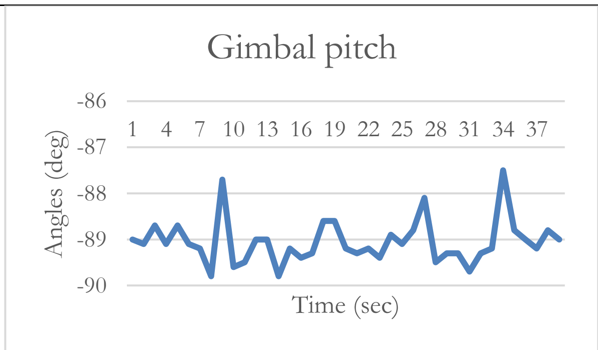

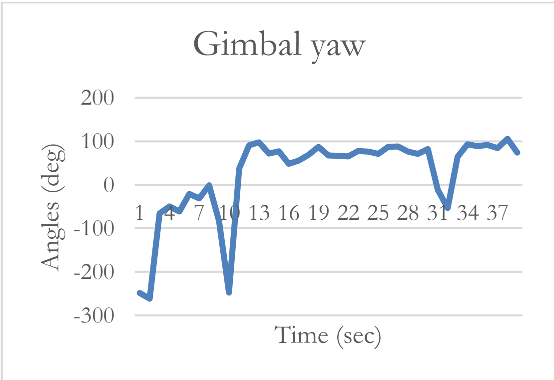

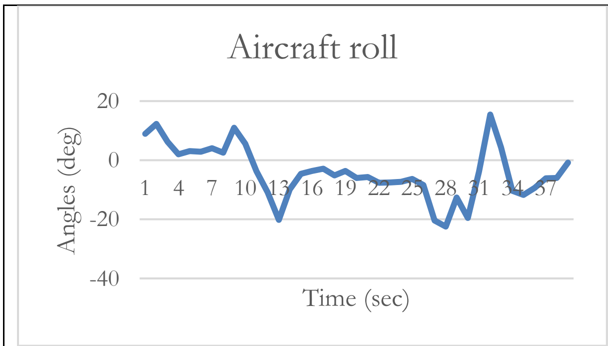

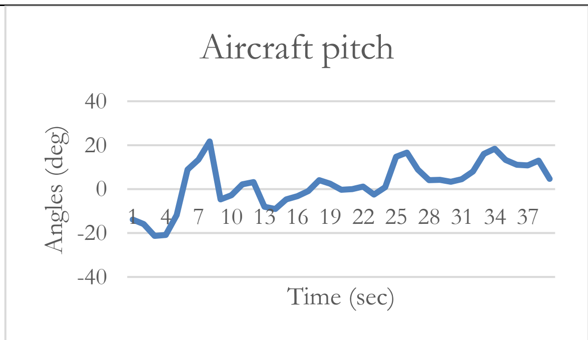

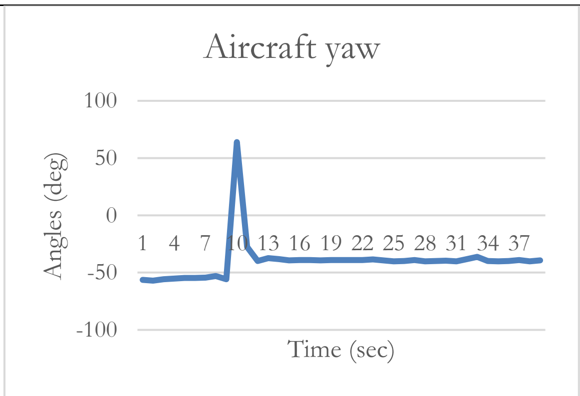
Aircraft yaw
100
50
0
-50
-100
Angles (deg)
1 4 7 10 13 16 19 22 25 28 31 34 37
Time (sec)

Flight 2

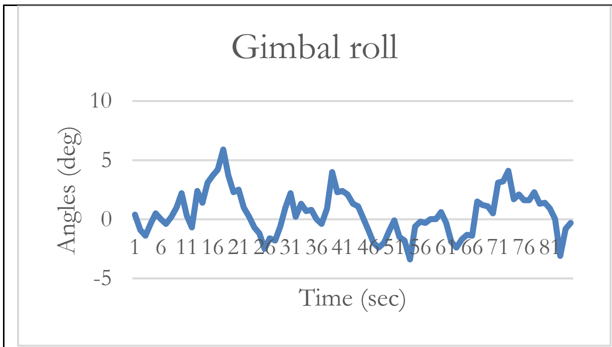
Gimbal roll
10
5
0
-5
Angles (deg)
1 6 11 16 21 26 31 36 41 46 51 56 61 66 71 76 81
Time (sec)

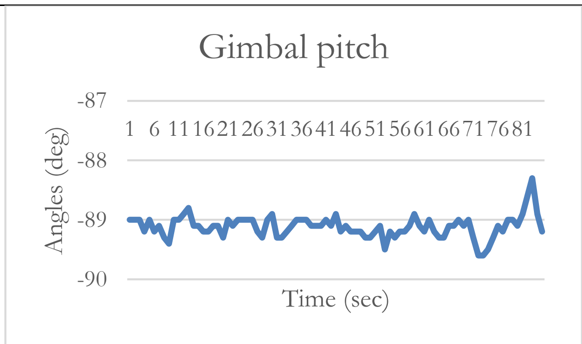
Gimbal pitch
-87
-88
-89
-90
Angles (deg)
1 6 11 16 21 26 31 36 41 46 51 56 61 66 71 76 81
Time (sec)

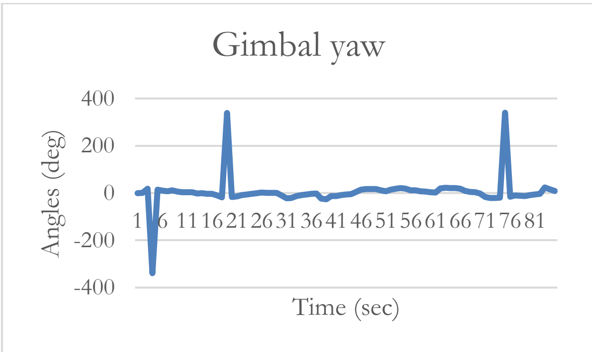
Gimbal yaw
400
200
0
-200
-400
Angles (deg)
1 6 11 16 21 26 31 36 41 46 51 56 61 66 71 76 81
Time (sec)

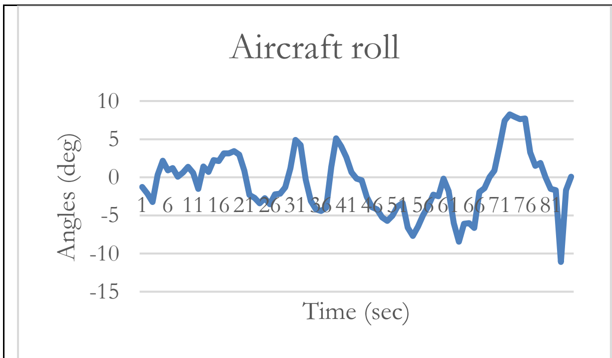
Aircraft roll
10
5
0
-5
-10
-15
Angles (deg)
1 6 11 16 21 26 31 36 41 46 51 56 61 66 71 76 81
Time (sec)

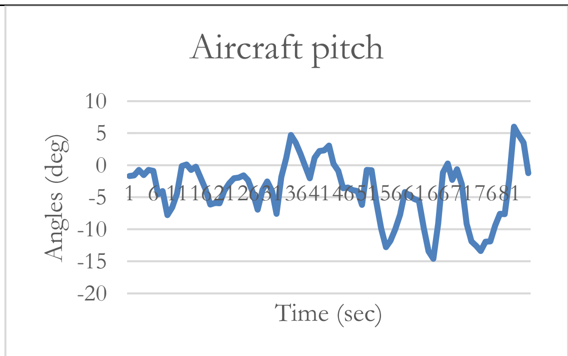
Aircraft pitch
10
5
0
-5
-10
-15
-20
Angles (deg)
1 6 11 16 21 26 31 36 41 46 51 56 61 66 71 76 81
Time (sec)

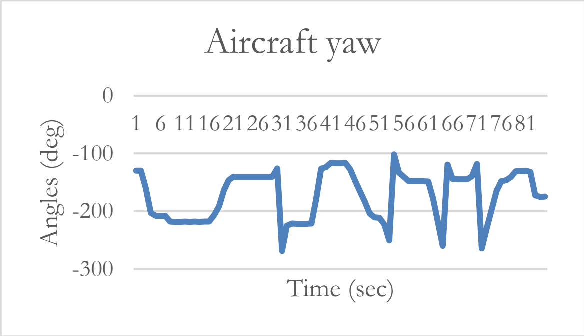
Aircraft yaw
0
-100
-200
-300
Angles (deg)
1 6 11 16 21 26 31 36 41 46 51 56 61 66 71 76 81
Time (sec)

Flight 3

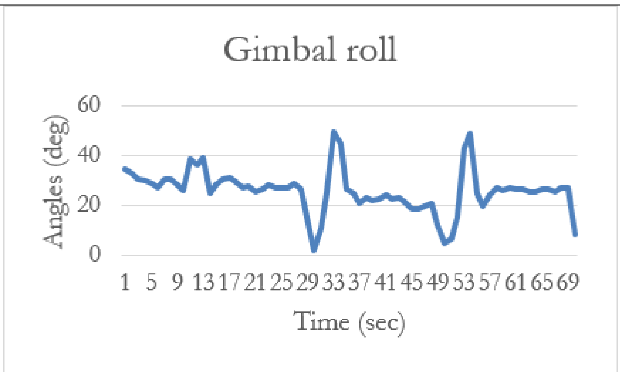
Gimbal roll
60
40
20
0
Angles (deg)
1 5 9 13 17 21 25 29 33 37 41 45 49 53 57 61 65 69
Time (sec)

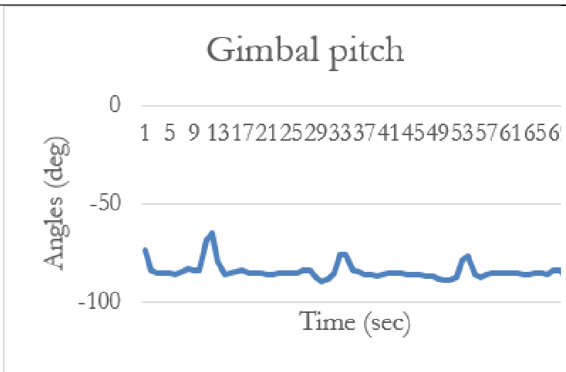
Gimbal pitch
0
-50
-100
Angles (deg)
Time (sec)

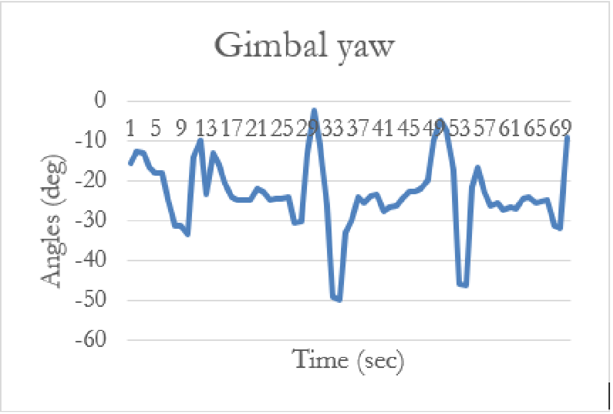
Gimbal yaw
0
-10
-20
-30
-40
-50
-60
Angles (deg)
Time (sec)

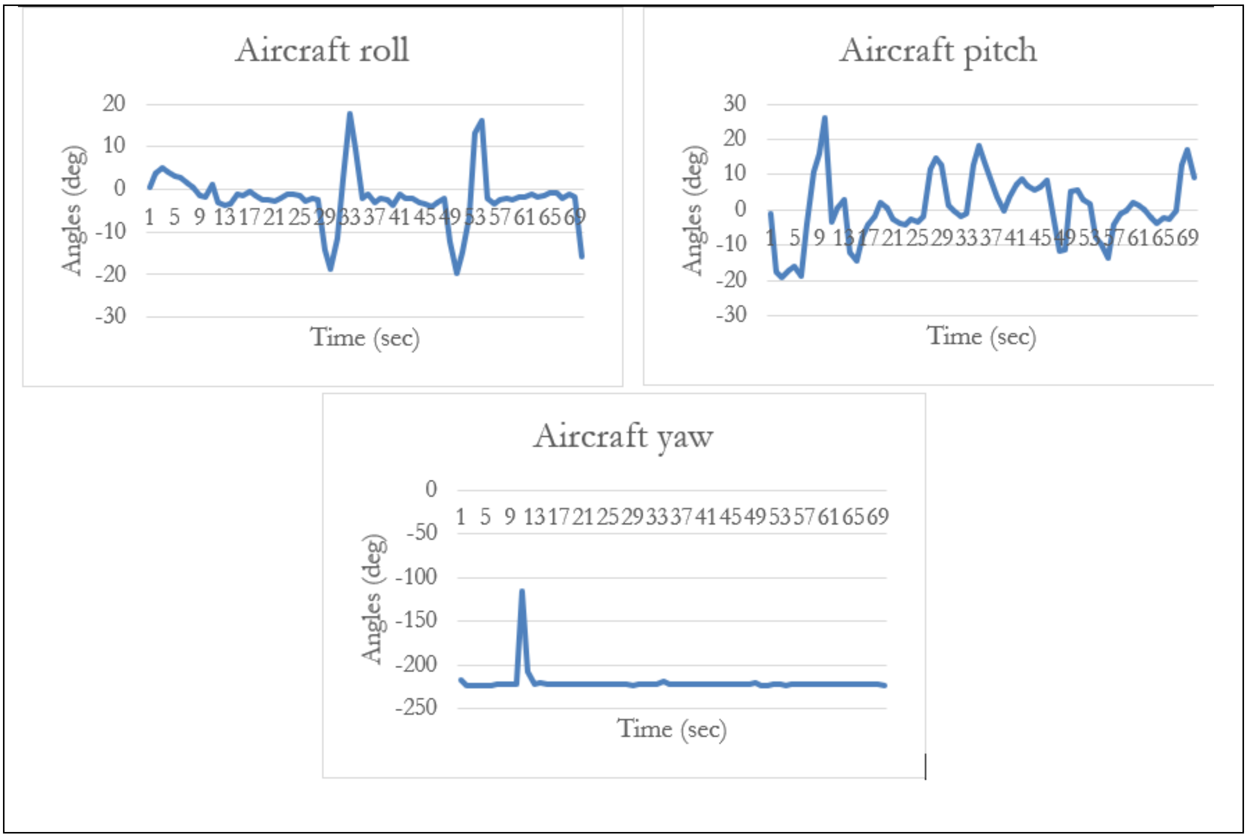

Appendix 3: Lever arm estimation procedure in matlab

```
%%%%% 3D rototranslation %%%%
Lever=xlsread('Lever
arm_F1.xlsx','Lever1','B2:J86');

a=1:85;
for a = 1:length (a);
    %%IMU angles
       ka=Lever(a,6);
phi=Lever(a,5);ome=Lever(a,4);
    %% Gimbal angles
    k=Lever(a,9); ph=Lever(a,8);om=Lever(a,7);
    X=Lever(a,1); Y=Lever(a,2); Z= Lever(a,3);
    Tk = [0;0;0.335]; Tl=[-0.11;0;0]; Tm=[0;0;-
0.195]; Tn=[0;0.09;0]; To=[0.19;0;0]; Tp=[0;-
0.12;0]; %translation vector
    %% Rotation of main IMU
```

```
    Rk_im = [cos(ka) -sin(ka) 0; sin(ka) cos(ka) 0;
0 0 1]; %count-clockwise
    Rp_im = [cos(phi) 0 sin(phi); 0 1 0; -sin(phi
0 cos(phi)];%count-clockwise
    Ro_im = [ 1 0 0; 0 cos(ome) -sin(ome); 0
sin(ome) cos(ome)]; %count-clockwise
    %% Rotation and translation (Gimbal imu)
    GPS = [X;Y;Z]; % GPS coordinate to be
translated in matrix format
    Rkap = [cos(k) -sin(k) 0; sin(k) cos(k) 0; 0 0
1]; %count-clockwise
    Rph = [cos(ph) 0 sin(ph); 0 1 0; -sin(ph)  0
cos(ph)];%count-clockwise
    Rom = [ 1 0 0; 0 cos(om) -sin(om); 0 sin(om)
cos(om)]; %count-clockwise

    %% Rototranslation (Rt) at the top of the
gimbal, point k
    R_x=Ro_im*Tk; % transformation around x axis
    R_y=Rp_im*R_x;%  transformation around y axis
    R_z=Rk_im*R_y;%  transformation around z axis
    Rtk=R_z+GPS;  % total transformation at point
k
    %% Rototranslation (Rt) at point L
    Rtl=Rkap*Tl+Rtk;

    %% Translation (Rt) at point M
    Rtm=Rtl+Tm;

    %% Rototranslation (Rt) at point N
    Rtn=Rom*Tn+Rtm;

    %% Translation (Rt) at point O
    Rto=Rtn+To;

    %% Rototranslation (Rt) at point P
    Rtp=Rph*Tp+Rto;% camera location at point p
    Lo=GPS-Rtp;
    IMU=[ka phi ome];
    Rb=eul2rotm(IMU);
```

```
    L=Rb*Lo;%GNSS RTK/camera offset/Lever arm
offset
    table(a,:)= [Rtp' L']; % displayes the results
in table format
   xlswrite('Lever
arm_F1.xlsx',table,'lever2','A2'); %writes the
results in excel file
 end
```

Appendix 4: Lever arm vector calculated per axis: